

# Local comparisons of tropospheric ozone: Vertical soundings at two neighbouring stations in Southern Bavaria

Thomas Trickl<sup>1</sup>, Martin Adelwart<sup>2</sup>, Dina Khordakova<sup>3</sup>, Ludwig Ries<sup>4</sup>, Christian Rolf<sup>5</sup>, Michael Sprenger<sup>5</sup>, Wolfgang Steinbrecht<sup>2</sup> and Hannes Vogelmann<sup>1</sup>

<sup>1</sup>Karlsruher Institut für Technologie, Institut für Meteorologie und Klimaforschung (IMK-IFU), Kreuzeckbahnstr. 19, D-82467 Garmisch-Partenkirchen, Germany

<sup>2</sup>Deutscher Wetterdienst, Meteorologisches Observatorium, Albin-Schwaiger-Weg 10, 82383 Hohenpeißenberg, Germany

<sup>3</sup>Forschungszentrum Jülich, IEK-7, Wilhelm-Johnen-Straße, 52425 Jülich, Germany

<sup>4</sup>Umweltbundesamt II 4.5, Plattform Zugspitze, GAW-Globalobservatorium Zugspitze-Hohenpeißenberg, Schneefernerhaus, 82475 Zugspitze, Germany

<sup>5</sup>Eidgenössische Technische Hochschule (ETH) Zürich, Institut für Atmosphäre und Klima, Universitätstraße 16, 8092 Zürich, Switzerland

*Correspondence to:* Dr. Thomas Trickl, thomas@trickl.de, Thomas-Knorr-Str. 47, D-82467 Garmisch-Partenkirchen, Germany; tel. +49-8821-50283; Dr. Hannes Vogelmann, hannes.vogelmann@kit.edu, Karlsruher Institut für Technologie, IMK-IFU, Kreuzeckbahnstr. 19, D-82467 Garmisch-Partenkirchen, Germany; tel: +49-8821-258

**Abstract.** In this study ozone profiles of the differential-absorption lidar at Garmisch-Partenkirchen are compared with those of ozone sondes of the Forschungszentrum Jülich and of the Meteorological Observatory Hohenpeißenberg (German Weather Service). The lidar measurements are quality assured by the highly accurate nearby in-situ ozone measurements at the Wank (1780 m a.s.l.) and Zugspitze (2962 m a.s.l.) summits and at the Global Atmosphere Watch station Schneefernerhaus (UFS, 2670 m a.s.l.), at distances of 9 km or less from the lidar. The mixing ratios of the lidar agree with those of the monitoring stations within  $\pm 3$  ppb, with a slight positive offset of  $0.6 \text{ ppb} \pm 0.6 \text{ ppb}$  (variation with year and station) conforming to the known  $-1.8\%$  calibration bias of the in-situ instruments. Side-by-side soundings of the lidar and electrochemical (ECC) sonde measurements in February 2019 by a team of the Forschungszentrum Jülich shows just small positive ozone offsets for the sonde ( $\leq 3.4$  ppb) and an agreement to within just  $\pm 2.5$  ppb in the troposphere after applying an altitude-independent bias correction to the sonde data, which we regard as the wintertime uncertainty of the lidar. We conclude that the recently published uncertainties of the lidar in the final configuration since 2012 are realistic and rather small for low to moderate ozone. Comparisons of the lidar with the Hohenpeißenberg routine measurements with Brewer-Mast sondes are more demanding because of the distance of 38 km between both sites implying significant ozone differences in some layers, particularly in summer. Our comparisons cover the three years September 2000 to August 2001, 2009 and 2018. A slight negative average offset ( $-3.64 \text{ ppb} \pm 7.5 \text{ ppb}$  (maximum of deviations)) of the sondes with respect to the lidar is found. Most sonde data could be improved in the troposphere by recalibration with the Zugspitze station data (until 2011 summit, afterwards UFS). This would not only remove the average offset, but also greatly reduce the variability of the individual offsets. The comparison for 2009 suggests a careful partial re-evaluation of the lidar measurements between 2007 and 2011 for altitudes above 6 km where occasionally a negative bias occurred.

*Key words:* Tropospheric ozone, ozone sonde, ozone lidar, differential absorption

## 41 1. Introduction

42 The development of tropospheric ozone has been studied over more than a century (e.g., Gaudel et al., 2018;  
43 Tarasick et al., 2019). For many decades, balloon-borne ozone sondes have been a primary work horse of ozone  
44 profiling. Their measurement principle is based on the oxidation of iodide (I<sup>-</sup>) to iodine (I<sub>2</sub>) by ozone in a wet-  
45 chemical potassium iodide (KI) cell. Between cathode and anode of the wet-chemical cell, the oxidation reaction  
46 drives an electrical current which can be measured (two electrons per ozone molecule). Recently, nearly all  
47 stations have used the so-called ECC (electro-chemical-cell) sonde type (Komhyr 1969; 1995), featuring two  
48 cells with different potassium iodide concentrations (anode and cathode cell). Only the Hohenpeißenberg station,  
49 discussed here, still uses the older-type Brewer-Mast sondes (Brewer and Milford, 1960), which uses one cell  
50 only (with a platinum cathode and a silver anode), and a less efficient pump design (Steinbrecht et al., 1998).  
51 Ozone sondes have been characterized in numerous studies, both in flight (e.g., Attmannspacher and Dütsch,  
52 1981; De Muer and Malcorps, 1984; Beekmann et al., 1994; Kerr et al., 1994; Jeannot et al., 2007; in recent  
53 years: Gaudel et al., 2015; Van Malderen et al., 2016; Deshler et al., 2017; Tarasick et al., 2021; Ancellet et al.,  
54 2022; Stauffer et al., 2022), and in a laboratory simulation chamber (Smit et al., 2007, 2014, 2021). Generally,  
55 the relative uncertainty of individual ECC soundings for ozone in the mid-latitude troposphere is about 5 to 10%  
56 (Logan et al., 2012; Smit et al., 2014; Tarasick et al., 2016, 2019). Following rigorous best practices, 5%  
57 accuracy can be achieved (Vömel et al., 2020; Smit et al., 2021; Tarasick et al., 2019; 2021). For Brewer-Mast  
58 soundings, the relative uncertainty in the troposphere is slightly higher, about 10 to 15% (Smit et al. 2014;  
59 Tarasick et al., 2016, 2019).

60 The ozone soundings at the Meteorological Observatory Hohenpeißenberg (MOHp) of the German Weather  
61 Service (Deutscher Wetterdienst, DWD) in Southern Bavaria have been routinely carried out since November  
62 1966, yielding one of the longest ozone-sonde time series. Brewer-Mast ozone sonde data tend to have a low  
63 bias above about 25 km altitude (Steinbrecht et al., 1998). In the troposphere, compared to ECC soundings,  
64 Tarasick et al. (2002, 2016) found a negative bias of about 20 % for ozone from Canadian Brewer-Mast  
65 soundings prior to 1980. European Brewer-Mast stations, however, have generally used a much more extensive  
66 preparation procedure for their sondes (Claude et al. 1987), and no significant tropospheric bias has been  
67 reported for their routine Brewer-Mast soundings (de Backer et al. 1998; Stübi et al. 2008; Logan et al., 2012), as  
68 well as in chamber experiments (Smit et al., 2014).

69 Routine measurements with ozone sondes yield time series free of a fair-weather sampling bias. However, the  
70 balloon ascents take place at intervals of several days. Ozone profiles at short intervals (less than one minute to  
71 several minutes) can be provided by lidar sounding, but are limited to clear atmospheric conditions. Lidar  
72 measurements can generate altitude-time curtain plots and, thus, give much better insight into the impact of  
73 atmospheric transport (e.g., Browell et al., 1987; Ancellet et al., 1991; Langford et al., 1996).

74 At IFU (Fraunhofer-Institut für Atmosphärische Umweltforschung; now: Karlsruher Institut für Technologie,  
75 IMK-IFU) in Garmisch-Partenkirchen (Germany), a differential-absorption lidar (DIAL) with a particularly wide  
76 operating range from next to the ground up to the upper troposphere was completed in 1990 in the framework of  
77 the TESLAS (Tropospheric Environmental Studies by Laser Sounding) subproject of EUROTRAC (TESLAS,  
78 1997; EUROTRAC, 1997, Kempfer et al., 1994). Subsequently, the system was applied for a full year (1991)  
79 within the TOR (Tropospheric Ozone Research; Kley et al., 1997) subproject of EUROTRAC (Carnuth et al.,  
80 2002). The operating range of this system was extended upwards to roughly 15 km in 1994 by introducing three-  
81 wavelength operation (Eisele et al., 1999). Due to its design, the IFU ozone DIAL features particularly low  
82 uncertainties.

83 Until 2003 the system was used for individual research projects. Between 2007 and 2018 routine measurements  
84 took place, parallel to lidar measurements of water vapour (Vogelmann and Trickl, 2008) and aerosol (Trickl et  
85 al., 2020b). The complementary information from these instruments has made possible a large number of  
86 investigations related to atmospheric transport. The IFU ozone DIAL was recently fully described by Trickl et al.  
87 (2020a).

88 The distance between MOHp and IFU is just 38 km which offers a good chance for comparisons. However, such  
89 a comparison must be made with care since the atmospheric variability is high on a rather small temporal and  
90 spatial scale (Vogelmann et al., 2011; 2015), mostly caused by the advection of air masses from rather different  
91 source region and altitudes, with different concentrations (e.g., Stohl and Trickl, 1999; Trickl et al., 2003; Trickl  
92 et al., 2011). The variability of the vertical distribution of ozone measurements rarely yields very strong  
93 concentration changes, but the concentration changes are extreme for water vapour. Our lidar measurements of  
94 water vapour exhibit a concentration span of more than two decades, with minima of the relative humidity (RH)  
95 clearly below 1 % in layers descending from the stratosphere (Trickl et al., 2014; 2015; 2016; Klanner et al.,  
96 2021).

97 Comparisons between the MOHp sonde and the IFU ozone lidar were made in the second half of the 1990s and  
98 in 2001, after the first upgrading of the lidar. A few of these comparisons in 1996 and 1997 were published by  
99 Eisele et al. (1997; 1999). For the six cases with supposedly sufficient air-mass matching a principal agreement  
100 in the middle and upper troposphere to within 5 ppb prevailed with occasional departures of the order of 10 ppb.  
101 Afterwards just routine comparisons with the nearby summit stations were made. Until 2010 the lidar results  
102 were compared with the long-term measurements at Wank and Zugspitze. Apart from occasional orographically  
103 induced deviations an agreement mostly to within  $\pm 2$  ppb was found. After these in-situ measurements were  
104 terminated the lidar measurements were compared with the ozone measurements at UFS. Mostly a similar  
105 agreement was found.

106 However, the need for a validation of the lidar also at higher altitudes has been obvious. Such an effort became  
107 more and more attractive with the growing technical performance of the system. In addition, hints on ozone  
108 differences between the Zugspitze (2962 m a.s.l.) in-situ data and the MOHp values (H. E. Scheel, personal  
109 communication around 2010) for 3 km a.s.l. have led to a revived interest in a thorough comparison. There have  
110 been speculations about an influence of a different air composition outside the mountains at low altitudes up to a  
111 few kilometres.

112 In this paper we first characterize the lidar performance by side-by-side ascents of ozone-sondes by a team of the  
113 Forschungszentrum Jülich (FZJ). Then, we give a statistical assessment for the measurements at IFU and MOHp  
114 for 2018. For this year we achieved the best coverage by DIAL measurements. This allows us to make an air-  
115 mass related data selection to improve the comparison. After the shutdown of the IFU summit stations in 2012,  
116 comparisons have been made exclusively with the Global Atmosphere Watch (GAW) routine in-situ  
117 measurements at the Schneefernerhaus high-altitude station (Umweltforschungsstation Schneefernerhaus, UFS,  
118 2671 m a.s.l.). UFS is located just below the Zugspitze summit. Finally, we also compare lidar and MOHp sonde  
119 for two earlier development phases of the lidar, for which ozone reference data at the local summit stations  
120 Wank (1780 m a.s.l.) and Zugspitze exist.

121  
122  
123

## 124 2. Methods

### 125 2.1 Brewer-Mast sonde system at Hohenpeißenberg

126 MOHp (975 m a.s.l., 47.80 N, 11.00 E) is located on an isolated mountain outside the Alps, 38 km to the north of  
127 IMK-IFU and 50 km to the south-west of Munich. Brewer-Mast ozone sondes have been launched on a regular  
128 basis since November 1966. The sondes undergo a rigorous preparation procedure (Claude et al. 1987), which  
129 has remained essentially unchanged since the early 1970s. From 1995 to 2005, Vaisala RS80 radiosondes and a  
130 Vaisala PC-CORA ground station have been used in combination with the ozone sondes. This was changed to  
131 Vaisala RS92 radiosondes and DigiCora III MW31 ground equipment in 2005, to MW41 ground station in 2018,  
132 and to Vaisala RS41 radiosondes in 2019. The standard processing does not subtract a background current, but  
133 ozone sondes with non-negligible background current on the ground (corresponding to 2.5 ppb ozone and more)  
134 are not flown. The background of most sondes launched is well below this threshold. Pump temperature is  
135 assumed to be constant at 300 K, which compensates to some degree for a too weak pump correction in the  
136 stratosphere (Steinbrecht et al. 1998). The time lag is comparable to that of ECC sondes (about 20 s; see Vömel  
137 et al., 2020). A time-lag correction is not applied, but this is not critical outside regions with steep ozone  
138 gradients since the corresponding vertical shift is just of the order of 0.1 km. Each ozone profile is adjusted by  
139 multiplication with an altitude-independent correction factor (typically around 1.08, standard deviation 5 %), so  
140 that the total ozone column estimated from the sounding (including an extrapolation above approximately 30  
141 km) matches the more accurate total ozone measurement from on-site Dobson or Brewer spectrometers, or from  
142 satellite instruments. This so-called “Dobson correction” generally improves that accuracy of the ozone sounding  
143 data in the stratosphere, but may introduce a small bias in the tropospheric data of some soundings (e.g., Stübi et  
144 al., 2008; Logan et al. 2012).

145 The MOHp ozone-sonde and radiosonde data are stored in the data base of the Network for the Detection of  
146 Atmospheric composition change (NDACC), from where they were imported for the study presented here.

### 147 2.2 ECC sonde system of the Forschungszentrum Jülich (FZJ)

148 A mobile balloon-borne sonde system of FZJ was operated at IMK-IFU (at 730 m a.s.l.), in close vicinity to the  
149 ozone DIAL (35 m), during the FIRMOS (Far Infrared Radiation Mobile Observation System) measurement  
150 campaign (Klanner et al., 2020; Palchetti et al., 2021; Di Natale, 2021; Belotti et al., 2023). Several balloons  
151 with cryogenic frostpoint hygrometers (CFH; Vömel et al., 2007; 2016), standard Vaisala RS-41-SGP  
152 radiosondes (Vaisala et al., 2019), En-Sci ECC ozone sondes (Komhyr et al., 1995; Smit et al., 2007) and  
153 COBALD backscatter sondes (Brabec, 2011) were launched. The data were transmitted to a ground station  
154 installed for this campaign at the Zugspitze summit. The combined balloon payload is well tested and regularly  
155 also used by the GCOS Reference Upper Air Network (GRUAN) (e.g., Dirksen et al., 2014).

156 We followed the standard operating procedures (SOP) of Smit et al. (2014) for the sonde preparation using a  
157 solution composition of 1 % and 1/10 (one-tenth) buffer for best results with sondes from the manufacturer En-  
158 Sci (Thompson et al., 2019).

159 For the analysis of the ECC data, the methods described by Vömel et al. (2020) are used, i.e., time lag correction  
160 and background current correction. The overall uncertainty of the ozone measurements of the ECC sondes is 5%.  
161 Due to the obstruction of the line of sight between launch site at IMK-IFU and the ground station at the  
162 summit by the Waxenstein mountain allowed data recording only from approximately 1500 m altitude upwards.  
163 Therefore, we used the estimated ECC background current from the sonde preparation one day before a flight as

164 starting value for the background correction instead of the actual measured profile from ground up to 1500 m.  
165 This results in an additional uncertainty in the lower part of the profile (2 to 3 km a.s.l.).

## 166 **2.4 IFU ozone DIAL system**

167 The ozone DIAL of IMK-IFU (Garmisch-Partenkirchen), located at 47.477 N, 11.064 E, and 740 m a.s.l., has  
168 been developed and optimized since 1988 (Kempfer et al., 1994; Trickl et al., 2020a). It is based on a krypton  
169 fluoride excimer laser, operated at 400 mJ per pulse (40 W) of narrowband radiation at 248.5 nm, two  
170 Newtonian receiving telescopes (diameter of the primary mirrors: 0.13 m and 0.5 m) and 1.1-m grating  
171 spectrographs for wavelength separation. Efficient stimulated Raman shifting in hydrogen and deuterium yields  
172 emission at the three operating wavelengths 277.2 nm, 291.8 nm and 313.2 nm. The shorter-wave spectral  
173 components are absorbed by ozone (“on” wavelengths), that at 313.2 nm (“off” or reference wavelength) is  
174 almost outside the absorption region of O<sub>3</sub>. The laser system is operated with a repetition rate of 99 Hz which  
175 allows a short data-acquisition time of just 41 s for the maximum number of 4096 laser shots accepted by the 24-  
176 bit memory of the electronics. More shots are advisable under noisy daytime conditions in summer, but a longer  
177 acquisition was prevented by laser issues.

178 The data evaluation is based on differentiating the backscatter signals, which is highly sensitive to the noise and  
179 imperfections of the raw data (stored in 7.5-m bins). Therefore, the generated ozone profiles are smoothed with a  
180 numerical filter. The noise fraction in the strongly decreasing backscatter signal grows with altitude. Thus, the  
181 smoothing interval must be dynamically enhanced towards the tropopause (yielding a vertical resolution 0.05 to  
182 0.5 km). The entire procedure is described in detail by Trickl et al. (2020a).

183 The shortwave 277.2-nm emission yields particularly accurate measurements, but the strong extinction of this  
184 radiation by ozone limits the range to about 8 km. The performance in the two 277.2-nm channels is robust with  
185 respect to minor misalignment, with uncertainties of about 2 to 4 ppb up to 5 km (the estimated uncertainties are  
186 listed in Table 4 of Trickl et al. (2020a)). This is not the case for 291.8 nm where the optical alignment must be  
187 controlled with care because of less tight focussing into the entrance slit of the far-field spectrograph. In  
188 addition, the 291.2-nm backscatter signal is three times noisier than that for 277.2-nm which necessitates  
189 stronger smoothing of the retrieved ozone profiles (Trickl et al., 2020a) For 5 to 8 km we specify uncertainties of  
190 3 to 7 ppb. The noise of the 313.2-nm signal becomes important at large distances. As a consequence, the  
191 uncertainty of the ozone mixing ratio can be become rather high in the upper troposphere and the tropopause  
192 region, in particular in summer due to the stronger loss of signal caused by the higher levels of ozone.  
193 Sometimes the uncertainty just below the tropopause can even exceed 10 ppb.

194 The DIAL data processing is made for different wavelength combinations (Eisele and Trickl, 2005). By  
195 comparing the resulting ozone profiles an internal quality control can be achieved. The optical alignment is  
196 optimized immediately after detecting an ozone mismatch in the first quicklook data evaluation. Just the laser  
197 beam overlap of the different wavelength components (Trickl et al., 2020a) and the beam pointing must be  
198 optimized.

199 The calibration of the ozone lidar measurements has been based from the very beginning (1991) on the accurate  
200 temperature-dependent ozone absorption cross sections of the University of Reims (Daumont et al., 1992;  
201 Malicet et al., 1995). These cross sections were verified for four wavelengths below 300 nm by Viillon et al.  
202 (2015) to within  $\pm 0.06$  %. In the presence of aerosol an aerosol correction is made with the algorithms of Eisele  
203 and Trickl (2005). This correction is rather robust for the wavelength pair 277 nm - 292 nm because of the strong  
204 absorption at the short “on” wavelength and the moderate wavelength difference (Völger et al., 1996).

205 Meteorological data for calculating density and temperature profiles are taken from the Munich radiosonde  
206 (station 10868). The retrieved 313-nm aerosol backscatter coefficients have been routinely stored in the data  
207 base of the European Aerosol Lidar Network (EARLINET) since 2007.

208 After repeated system upgrading the final performance of the lidar was reached in late 2012. In the absence of  
209 aerosol the far-field ozone could be evaluated with high reliability from the 291.9-nm signal alone, after  
210 precisely modelling the air number density from radiosonde data (Trickl et al., 2020). In this way the daytime  
211 noise caused by the high solar background in the 313-nm reference profiles in summer could frequently be  
212 avoided.

213 During the final decade of the lidar operation a fitting procedure was applied in noisy situations in the upper  
214 troposphere (i.e., under high-ozone conditions in summer). This procedure reduces unrealistic curvature of ozone  
215 structures caused by enhanced data smoothing, and, thus, abrupt concentration changes (in particular at the  
216 tropopause) visible in the raw data are reproduced in the mixing ratio.

217 From 1991 to 2003 the DIAL was operated for focussed research projects. Routine measurements took place  
218 from 2007 to 2018, until 2015 parallel to measurements with a water-vapour DIAL (Trickl et al., 2014, 2015,  
219 2016, 2020b). In 2012 the highest data quality was finally reached, which included significant improvements for  
220 the near-field telescope (Trickl et al., 2020a). Thus, the conditions for a meaningful system validation were  
221 obtained. The operation was discontinued in February 2019, after the retirement of the first author of this paper.

## 222 **2.5 High-elevation surface observations**

223 Quality-assured ozone measurements at the summit stations Wank (1780 m a.s.l., 7.0 km to the north-east of  
224 IMK-IFU, 47.511° N, 11.141° E) and Zugspitze (2962 m a.s.l., 8.4 km to the south-west of IMK-IFU, 47.421° N,  
225 10.986° E) took place from 1978 to 2012. Since the 1990s, two or three TE 49 ozone analysers (Thermo  
226 Environmental Instruments, USA) were operated simultaneously at each station. These instruments are based on  
227 ultraviolet (UV) absorption at 253.65 nm. Several comparisons using transfer standards (O<sub>3</sub> calibrators TE 49  
228 PS) were made with the World Meteorological Organization (WMO) Global Atmosphere Watch (GAW)  
229 reference instrument kept at the WMO/GAW calibration centre operated by EMPA, Switzerland (Klausen et al.,  
230 2003). The most recent comparison was conducted in June 2006 and confirmed that the Zugspitze O<sub>3</sub> data are on  
231 the GAW scale.

232 Apart from the two mountain stations measurements were performed also at IFU at about 740 m a.s.l. (47.477°  
233 N, 11.064° E). This laboratory was adjacent to that of the ozone DIAL.

234 At UFS (0.70 km to the south-east of Zugspitze, 47.417°, 10.980° E) ozone has been continuously measured  
235 since 2002 by a team of the German Environment Agency (Umweltbundesamt, UBA) using TEI 49i instruments  
236 (Thermo Electron Corporation). The gas inlet is at 2671 m a.s.l. For weekly and monthly calibration of the ozone  
237 measurements a TEI 49C-PS station ozone calibrator was applied. This primary standard was annually adjusted  
238 to the German ozone standard operated by UBA (UBA 204 SRP#29) that was adjusted via BIPM (Bureau  
239 International des Poids et Mesures) in Paris to the NIST ozone reference standard of GAW. The measurements  
240 were supported by a second instrument (Horiba APOA-370) which is equivalent to the TEI-49i. GAW  
241 performance audits at the station for surface ozone took place in 2001, 2006, 2011 and 2020 (Zellweger et al.,  
242 2001; 2006; 2011; 2020).

243 The uncertainty of the in-situ ozone measurements is  $\pm 0.5$  ppb with respect to the WMO standard (Hearn et al.,  
244 1961). This fulfills the GAW requirement.

245 The ozone data for all sites are stored at half-hour intervals. The times are specified for the end of the averaging  
246 interval in Central European Time (CET, = UTC + 1 h). 1-h averages for the Zugspitze stations were made  
247 available to the World Data Center and the TOAR data base (Schultz et al., 2017). In the present study we use  
248 data at half-hour time resolution. The ozone series at the two Zugspitze sites have been discussed on two recent  
249 scientific studies (1970 to 2020; Parrish et al., 2019; Trickl et al., 2023).

## 250 **2.6 LAGRANTO Trajectories**

251 Fifteen-day backward trajectories were calculated with the Lagrangian Analysis tool (LAGRANTO; Sprenger  
252 and Wernli, 2015; Wernli and Davies 1997). The driving wind fields are obtained from the ERA5 reanalysis  
253 dataset (Hersbach et al., 2020), which we interpolated to a 0.5° latitude/longitude grid, and on 137 vertical hybrid  
254 levels. The input ERA5 data are available at a one-hour temporal resolution; the output positions of the  
255 trajectories are written at 15-min time interval to allow for a more refined analysis. The start coordinates of the  
256 backward trajectories are 11.064 E, 47.477 N, and the start altitudes match the altitudes of interest in the  
257 soundings (see Sect. 4). The start times of the trajectories correspond to the sounding times within five minutes.  
258 Finally, the start times are also shifted by several hours relative to the sounding time to assess the sensitivity of  
259 the trajectory calculation on time.

## 260 **3. Results**

261 The main problem in comparing vertical-sounding instruments is illustrated in Fig. 1 which shows several ozone  
262 measurements at Garmisch-Partenkirchen and Hohenpeißenberg in the morning of 2 October 2017. The vertical  
263 distributions during that period are characterized by a descending stratospheric intrusion layer (see low relative  
264 humidity) of rapidly diminishing width and significant changes at all altitudes on a short time scale. This reveals  
265 a considerable spatial inhomogeneity of the air mass. The approximate agreement of lidar and Hohenpeißenberg  
266 ozone sonde before 6:00 CET is, thus, fortuitous. Different air masses must be assumed at different altitudes  
267 must be assumed as indicated by matching of the sonde ozone with lidar measurements at different times. The  
268 spatial and temporal requirements for comparisons can be even of the order of 1 km and 15 min at times (see  
269 Introduction).

### 270 **3.1 Comparisons of the IFU ozone lidar and the Jülich ECC sonde**

271 An optimum lidar validation became possible in early 2019. On 5 and 6 February 2019 a side-by-side instrument  
272 comparison took place at Garmisch-Partenkirchen as a contribution to the FIRMOS validation project of the  
273 European Space Agency. Two of the three balloons launched on 5 February were equipped with ozone sondes,  
274 while both balloons on 6 February carried an ozone sonde. The ascents took place during night-time because of  
275 comparisons of the CFH sondes with the water-vapour channel of the UFS Raman lidar that provides humidity  
276 profiles up to at least 20 km (Klanner et al. 2021).

277 The first night of the campaign was clear. The conditions for the comparison were excellent: the sondes rose  
278 almost vertically up to 8.5 km and then slowly drifted to the south-east (Innsbruck), ideal for the tropospheric  
279 comparison. The balloons stayed within 20 km distance from IMK-IFU up to the tropopause (12.8 km a.s.l.) and  
280 remained within 30 km up to 20 km a.s.l.

281 The launch times of the balloons were 18:03 CET (ascent to 16.147 km), 19:03 CET (29.475 km), and 23:00  
282 CET (29.469 km).

283 In Fig. 2 we present the results of the four comparisons made. The measurements of lidar, ECC sonde and in-situ  
284 sensor at UFS on 5 and 6 February are in outstanding agreement provided that a correction of a small altitude-  
285 independent positive offset (not shown) is applied to the (uncalibrated) sonde ozone. We are highly content that  
286 the agreement stays exceptional even in the upper troposphere considering the low differential absorption for the  
287 wavelength pair 292 nm – 313 nm typically used above 6 km that implies a high sensitivity to potential technical  
288 imperfection.

289 In addition, we show in Fig. 2 the results of three humidity measurements with the UFS Raman lidar slightly  
290 revised with respect to Klanner et al. (2021). For comparison, we added the water-vapour mixing ratios (MRs)  
291 for the corresponding CFH sonde ascents of FZJ. The MRs indicate a high variability of the air composition on  
292 both days, up to 7 km, with several rapidly changing dry layers. The variability grows with time, as can also be  
293 concluded from the differences of Raman lidar and CFH sonde, caused by the 1-h measurement duration of the  
294 lidar needed for good stratospheric data quality. Although the vertical concentration change is much less  
295 pronounced in the ozone profiles, it is obvious that a good air-mass matching by the side-by-side ozone  
296 soundings at IMK-IFU is crucial for the quality of the comparison achieved.

297 On 6 February the quality of the lidar retrievals was deteriorated by a layer of cirrus clouds above 9 km, which  
298 required an aerosol correction. An increased level of ozone in this layer is remarkable, but is verified by the  
299 sonde. By contrast, Reichardt et al. (1996) reported full ozone depletion in a cirrus layer that we traced back to  
300 the surface of the Pacific Ocean where ozone destruction can be assumed to prevail (Kley et al., 1996). The  
301 fourth comparison shows less perfect agreement because the lidar measurements ended at 19:00 CET, hours  
302 before the last sonde ascent. This was the final measurement of the DIAL before its operation was terminated  
303 after almost three decades.

304 Ozone profiles are also available for the descent of the balloons. The descents took place over Northern Italy and  
305 intersected different air masses. As a consequence, strong discrepancies are seen, and we do not include these  
306 data.

307 For quantifying the quality of the lidar measurements we took just the first three comparisons. In order to  
308 evaluate the agreement of the vertical profiles of the two systems in structure we determined the average sonde  
309 offsets up to about 6 km (i.e., in the range of the best lidar performance), yielding values between +0.53 and +3.4  
310 ppb. These offsets were first subtracted from the sonde ozone profiles. Then, the differences between the  
311 corrected sonde and the lidar data were formed at intervals of 52.5 m, for the first comparison on 6 February just  
312 up to 8.7 km. Finally, we averaged these differences (Fig. 3). The differences up to 9.2 km stay within  $\pm 2.5$  ppb  
313 (about  $\pm 5$  %). This is approximately matches the performance of the lidar at the station altitudes and now  
314 characterizes the winter-time specifications of the lidar also in the free troposphere after 2011. This result  
315 justifies to use the lidar as a quality standard in the comparisons with the MOHp Brewer-Mast sondes described  
316 in the following sections.

317 The quality of the comparison shown in this section benefits from low to moderate ozone densities during the  
318 cold season, which ensures limited absorption of the laser radiation within the troposphere. In Sect. 3.2 we assess  
319 the performance for all seasons.

### 320 **3.2 Comparison of MOHp ozone soundings with IFU lidar and in-situ measurements for 2018**

321 The routine measurements with the IFU ozone DIAL exhibit rather different annual coverages, with gaps due to  
322 system damage or upgrading periods. Starting in late 2012 the final technical performance was reached.  
323 Retrieval strategies have been further improved. The best coverage of a single year was achieved in 2018 with a



324 total of 587 measurements and 16 (March) to 79 (September) measurements per month. Therefore, we use this  
325 year for a thorough comparison with the MOHp ozone sonde.

326 The sonde ascents at MOHp usually take place around 6:00 CET on Monday, Wednesday and Friday, in summer  
327 just on Monday and Wednesday. We found a total of 46 of these days on which early-morning lidar  
328 measurements exist, not later than around 10:00 CET. On 36 of these days MOHp soundings are available.  
329 Thirteen of the days provided particularly good conditions with favourable temporal proximity. In the figures  
330 shown in this paper we eliminated ozone profiles for times later than 10:00 CET during a given day.

### 331 *Winter*

332 During the cold parts of the year the comparisons usually exhibit better quality. This is explained by less  
333 structure in the ozone vertical distributions and a wider operating range of the lidar due to the low ozone level  
334 allowing for a higher, less noisy far-field signal. This was already demonstrated in the previous section. For the  
335 2018 comparison we give one example in Fig. 4. The lidar mixing ratio is of the order of 45 ppb, verified by the  
336 measurements at UFS (2660 m a.s.l.). There is an obvious constant offset of the sonde mixing ratio with respect  
337 to the lidar ozone profile. After adding 5.8 ppb the sonde results (cyan curve) match the lidar values well for  
338 altitudes above 2.1 km. Just below the tropopause there is a minor discrepancy that could be either due to the  
339 higher uncertainty of the lidar measurement at these altitudes or air-mass differences.

### 340 *Summer*

341 During the warm season the ozone distribution in the middle and upper troposphere shows structured maxima  
342 caused by long-range transport, in particular STT (stratosphere-to-tropopause transport) layers (Trickl et al.,  
343 2020b). In this altitude range a summer maximum of STT exists. Usually, these structures do not perfectly match  
344 for both sites. An example for 9 July 2018 is shown in Fig. 5.

345 Figure 5 shows good agreement in structure between the soundings at both sites up to 9 km. Again, despite the  
346 pronounced ozone layering, the agreement was improved on the absolute scale by adding an altitude-independent  
347 correction to the sonde values (6 ppb). Thus, this approach was applied throughout our study. The offset is  
348 usually determined up to 6 km due to the reliable performance of the 277-nm-313-nm measurements, but the  
349 agreement is mostly reasonable also to higher altitudes. After shifting the sonde mixing ratio we can estimate the  
350 uncertainty of the lidar measurements.

351 The elevated ozone between 3.3 km and 4.7 km can be explained by a stratospheric air intrusion, as is verified by  
352 the low RH. In the upper troposphere the agreement deteriorates, but at least the increase of ozone with altitude  
353 is seen in all profiles up to about 12 km. The ozone minimum around 13 km is just seen in the lidar data, with  
354 just a small ozone dip in the sonde profile. It is unreasonable to ascribe this considerable discrepancy to a  
355 temporary technical problem in such a limited altitude range. This example documents the difficulty of  
356 quantitative comparisons of tropospheric ozone even on a horizontal scale of just 38 km.

357 In order to clarify the origin of the difference of the ozone mixing ratio in the upper troposphere we calculated  
358 backward trajectories with the HYSPLIT model (<http://ready.arl.noaa.gov/HYSPLIT.php>; Draxler and Hess,  
359 1998; Stein et al., 2015). These trajectories reveal northerly advection which implies a southward drift of the  
360 sonde towards the lidar during the ascent. In the upper troposphere they did not fully explain the observations  
361 within the limited maximum backward time span of 315 h. This includes “ensemble” trajectory bundles that  
362 visualize a wider range of source regions.

363 Therefore, the trajectory calculations were extended to 350 h by using the LAGRANTO model for full-hour start  
364 times between 3:00 CET and 8:00 CET, initiated in the low-ozone range in the upper troposphere. Results for  
365 start times of 7:00 CET and 8:00 CET are shown in Figs. 6 and 7. Up to a start time of 4:00 CET the trajectories  
366 stayed almost completely at high altitudes. At 5:00 CET three of the trajectories ended in the lower troposphere  
367 above the subtropical Pacific near a longitude of 180°, first sign of an air-mass change. Later (Figs. 6 and 7) we  
368 see a clear influence of a Pacific source.

369 The low ozone level in the boundary layer above (sub)tropical oceans is well known (Eisele et al., 1999; Grant et  
370 al., 2000; Trickl et al., 2003), in particular over the Pacific (Kley et al., 1996; Davies et al., 1998). In this way,  
371 the lidar observations on 9 July 2018 can be understood. The launch time of the MOHp ozone sonde, 5:42 CET,  
372 is between the two lidar measurements. However, a delay is caused during the ascent which makes a quantitative  
373 understanding difficult.

374 The moderate sonde RH above 12.3 km indicates a potential admixture of aged stratospheric air in this altitude  
375 range above MOHp which would explain the high ozone mixing ratios of more than 120 ppb.

376 Figures 5 and 8 show a rather constant negative ozone offset of the sonde profiles. The ozone profiles can be  
377 brought into much better agreement by upward shifts by 6 ppb and 10 ppb, respectively. In Fig. 9 one sees one of  
378 the very rare cases of an ozone mismatch between sonde and lidar up to elevations clearly above the mountain  
379 sites (1 km above the Zugspitze summit). We did not shift the MOHp profile (e.g., by 3 ppb) to reduce the  
380 mismatch since this would reduce the good agreement above 4 km.

### 381 *Offsets*

382 The offsets of the MOHp data from the DIAL profiles were evaluated for all 36 comparison days. The result of  
383 the statistical assessment is displayed in Fig. 10 where also the differences between the lidar results for 2671 m  
384 a.s.l. and the GAW measurements at UFS are shown. Just one case was eliminated in the comparison of lidar and  
385 UFS: A strong negative shift of -7 ppb can be seen in Fig. 5 where UFS is located in the falling edge of a high-  
386 ozone range.

387 As found for the lidar measurements over many years (examples: Trickl et al., 2014, 2015, 2016, 2020b) the  
388 lidar ozone agrees with that at UFS to within  $\pm 3$  ppb. The agreement would perhaps be better if orographic  
389 vertical displacements and air flows on the ozone profiles would be considered (Carnuth et al., 2000; 2002; Yuan  
390 et al., 2019; Trickl et al., 2020a). The average difference between lidar and UFS for 2018 (blue horizontal line in  
391 Fig. 10) is  $0.736 \text{ ppb} \pm 1.46 \text{ ppb}$  (standard deviation). A positive offset had also been found for an earlier four-  
392 day comparison with the Zugspitze summit, but with even higher uncertainty (Trickl et al., 2020a). A positive  
393 offset of this size could be expected from the highly accurate cross-section measurements of Viallon et al.  
394 (2015), who determined a negative bias of 1.8 % of in-situ data calibrated with the WMO standard. This relative  
395 difference becomes more important on the absolute scale in summer than in winter because of the higher ozone  
396 values. However, the statistical noise of the differences is too high to allow resolving such an effect.

397 The offsets between the MOHp sonde and the lidar, again preferentially determined in the range up to 6 km, are  
398 substantially higher (red filled squares in Fig. 10). The offsets of the ozone sondes range from -12 ppb to +4  
399 ppb, with an average of  $-3.77 \text{ ppb}$  (red horizontal line in Fig. 10) and a standard deviation of 4.22 ppb.

400 We exclude the lowest altitudes from the comparison where obvious differences in ozone exist, e.g., due to local  
401 night-time ozone depletion effects. It is important to note that just in seven cases of the 36 comparisons for 2018  
402 lower ozone in the sonde profiles reached up to more than 2.67 km (UFS), in three cases to more than 3 km

403 (Zugspitze summit). We conclude that differences between the Zugspitze sites and the MOHp sonde are mostly  
404 related to sonde calibration issues and not to differences in air-composition as suspected earlier.

### 405 *Differences*

406 In order to determine the quality of the lidar measurements we show in the three panels of Fig. 11 average  
407 differences between lidar and offset-corrected MOHp sonde data as a function of altitude and for three different  
408 ozone conditions, roughly below 50 ppb (low ozone; top panel), between 50 to 70 ppb (moderate ozone; second  
409 panel) and more than 70 ppb (high ozone; bottom panel), respectively. On a given day, the lidar ozone profiles  
410 agreeing best with the MOHp profile was taken. We also give the percentages of the averages with respect to the  
411 offset-corrected sonde ozone. At high altitudes the sonde ozone is a more useful reference than the lidar in the  
412 case of high ozone because of the considerable absolute uncertainty caused by the loss of laser radiation by  
413 absorption in ozone.

414 For winter-type conditions (top panel) the six examples averaged do not exhibit a significant vertical ozone  
415 structure which made the analysis straight forward and yields astonishingly small average differences between  
416  $\pm 1$  ppb and  $\pm 3$  ppb. For moderate ozone (second panel) and high ozone (bottom panel), mostly during the warm  
417 season, the vertical distributions are more complex with changes on a time scale of even less than one hour.  
418 Here, we eliminated the data for a few pronounced ozone peaks and dips that differed at both stations. The six  
419 high-ozone cases were restricted to July and August.

420 The averaged distributions of the differences exhibit oscillations. These oscillations were analysed for coherency  
421 (not shown), but no systematic behaviour was identified. Thus, we ascribe the structure to noise. The noise  
422 contains both an atmospheric and an instrumental component.

423 Beyond the days and years of the comparison there are occasionally extreme cases with 100 to 150 ppb in the  
424 middle and upper troposphere. This can lead to lidar uncertainties even up to more than 20 ppb during daytime,  
425 also because the raw signal becomes comparable with the additional solar background noise. In the severest  
426 cases the stratospheric ozone rise cannot be seen in the lidar data during daytime, and the ozone profile is cut off  
427 in the upper troposphere for archiving.

428 The analyses for 2018 do not reveal a significant bias between the lidar values and the offset-corrected sonde  
429 data (based on the numbers underlying Fig. 10). The maximum noise excursions can be interpreted as maximum  
430 combined uncertainties of lidar and corrected sonde in a given altitude range (slightly overestimated due  
431 atmospheric differences in ozone between both sites). The results of this analysis confirm the estimates in Table  
432 4 of Trickl et al. (2020a).

### 433 **3.3 Comparisons of MOHp sonde, IFU lidar and in-situ measurements at summits in 2009**

434 The results in Sect. 3.2 suggested to look also at a few earlier years. We select 2009 from the period of routine  
435 measurements as another year of comparison. The lidar raw data were noisier than for the period after 2012 and  
436 a tiny electronic ringing effect had to be removed mathematically. Thus, the uncertainties of the ozone profiles  
437 above 6 km are higher than after the final system upgrading in 2012, particularly in summer. As a consequence,  
438 a lidar validation is desirable at least for the upper troposphere. More importantly, in 2009 high-quality ozone  
439 data still exist for the summit stations Wank (1780 m a.s.l.) and Zugspitze (2962 m a.s.l.). These stations benefit  
440 from more frequent direct advection compared with UFS.

441 In 2009 the lidar was operated just until October which, nevertheless, allows us to make a reasonable number of  
442 comparisons with MOHp. The operation was stopped afterwards since there were more and more cases of single-

443 bit errors in channel 5 of the transient digitizer system which had to be sent for repair. These errors induced  
444 unrealistic data in the upper troposphere.

445 We identified a total of 23 days suitable for comparisons. On just eight of these days lidar measurements were  
446 made in optimum temporal proximity. We find more deviations in the profiles than for 2018. In part, this can be  
447 explained by atmospheric variability and insufficient air-mass matching. In addition, as mentioned, the raw data  
448 of the lidar are noisier and some weak ringing had to be removed. This caused elevated uncertainties above 6  
449 km. Nevertheless, the data allowed us to determine offsets for the MOHp ozone profiles, after verifying the data  
450 quality of the lidar with the Zugspitze and Wank in-situ ozone.

451 In Fig. 12 we show the results of the analysis for 2009. The difference between IFU DIAL and Zugspitze is  
452  $-0.165 \text{ ppb} \pm 1.36 \text{ ppb}$  (standard deviation), between DIAL and Wank  $+0.714 \text{ ppb} \pm 1.20 \text{ ppb}$ . The DIAL ozone  
453 below the Wank altitude is increasingly uncertain because of alignment issues of the near-field telescope. In an  
454 earlier comparison for May 1999 (Trickl et al., 2020a) we selected a lower altitude in the DIAL data (2786 m)  
455 and found better agreement, but, still, a slight positive offset with respect to the station. This is not attempted  
456 here, although we can see the effect of orographic lifting in some examples.

457 For 2009 the offsets between DIAL and MOHp sondes were determined primarily by between 2 and 5 km. The  
458 sonde offset obtained in this way is, again, negative on average ( $-1.500 \text{ ppb}$ ), with a standard deviation of 2.67  
459 ppb, both being less pronounced than in 2018.

460 Figure 13 shows a comparison on 12 January 2009, demonstrating excellent agreement between both systems,  
461 except for the upper troposphere and lower stratosphere. In this case, the first lidar measurement took place at  
462 9:20 CET, i.e., substantially later than the sonde ascent. Thus, the comparison has its limits. In the morning of 12  
463 January westerly advection was revealed by HYSPLIT backward trajectories above at 7 km a.s.l.. This air mass  
464 originated below 2 km over the subtropical Atlantic. This could explain the slightly lower ozone level around  
465 this altitude in the lidar results.

466 Another interesting example is August 17 (Fig. 14). The agreement between lidar and ozone sonde is highly  
467 satisfactory up to 5.4 km and quite reasonable up to 10 km. However, between 10 km and 14.5 km the lidar  
468 ozone is extremely low, in contrast to the sonde data. The pronounced ozone increase in the sonde data above 10  
469 km is difficult to explain since the elevated RH values suggest neither a low tropopause nor the presence of a  
470 stratospheric intrusion that typically features RH values of a few per cent at most (Trickl et al., 2014; 2015;  
471 2016). On the other hand, the ozone peak above IMK-IFU descending roughly from 10 to 8 km is attributed by  
472 HYSPLIT calculations to subsiding air, indicating the presence of an intrusion layer. It is interesting that the  
473 rather short delay of the lidar measurements (7:00 CET to 9:15 CET) with respect to the sonde ascent (launch  
474 time 5:57 CET) can result in such a considerable difference.

475 Again, 350-h LAGRANTO trajectories were calculated for start times above IMK-IFU between 3:00 CET and  
476 8:00 CET (interval: 1 h) and start altitudes within the low-ozone layer. Until 6:00 CET the influence of marine  
477 boundary layers is almost absent. Afterwards, the trajectories reveal a growing import from the first 600 m above  
478 the subtropical Atlantic Ocean. In Fig. 15 the LAGRANTO results for 8:00 CET are shown.

479 In many cases the lidar seems to exhibit a negative bias with respect to the sondes in the upper troposphere. It is  
480 advisable to re-examine a major part of the data between 2007 and 2011, also including strategies developed  
481 later. For example, an exponential decay of the analogue signal was identified with the much lower noise of the  
482 final setup (Trickl et al., 2020a) which must be addressed.

483

### 484 3.4 Comparisons of MOHp sonde, IFU lidar and in-situ measurements summits in 2000 and 2001

485 The period September 2000 to August 2001 is suitable for another comparison when a large number of STT-  
486 related measurement series were made as a contribution to the STACCATO project (Stohl et al., 2003;  
487 examples: Trickl et al., 2003; 2010; 2011; Zanis et al., 2003). These measurements were made with the noisier  
488 detection electronics of Eisele et al. (1999), but had the advantage that single-photon counting was used for the  
489 “solar blind” “on” detection channels which added linearity above 5 km (starting in spring 1997). The counting  
490 system could no longer be computer controlled after 2006. A new one was installed after highly positive results  
491 in other IFU lidar systems (Klanner et al., 2021) in autumn 2018, too late for this comparison effort.

492 The focus on STT during the STACCATO period made the comparisons a challenge because of the pronounced  
493 layering. However, on 11 of the useful 20 days of comparison there was reasonable temporal proximity, due to  
494 running long time series. The agreement between the lidar and the MOHp sonde was much better than expected  
495 in the entire free troposphere. The agreement (after offset-correcting the MOHp profiles) is almost perfect during  
496 the cold season. But also under high-ozone conditions the comparisons do not reveal systematic differences  
497 beyond the sonde offsets.

498 Two examples for elevated ozone are shown in Figs. 16 and 17. The good comparisons support our earlier work  
499 (Trickl et al., 2003, 2010), and we tend to ascribe this to the satisfactory performance of the single-photon  
500 counting system.

501 For several weeks a strange ozone rise towards the ground was observed in the lidar data below 1.5 km. This  
502 effect disappeared after realigning the near-field telescope and the normal early-morning ozone drop returned.

503 However, the offsets of the MOHp mixing ratios necessary to achieve good agreement are, again, quite  
504 substantial (Fig. 18). Due to the larger system noise during that period also the differences between lidar and the  
505 stations are higher than those in the preceding sections, and comparable with those of the mentioned four-day  
506 comparison for May 1999 (Trickl et al., 2020a). The statistical analysis yields the following average differences  
507 and standard deviations:

508 IFU DIAL – Zugspitze:	1.22 ppb ± 1.81 ppb
509 IFU DIAL – Wank	–0.15 ppb ± 2.26 ppb
510 MOHp – IFU DIAL	–5.88 ppb ± 3.35 ppb

### 511 4. Discussion and Conclusions

512 For some time tropospheric differential-absorption ozone lidar systems had a bad reputation: The method is  
513 highly sensitive to imperfections in the signal acquisition since the ozone number density is obtained by  
514 differentiating the backscatter signals. In addition, a lidar covering the entire troposphere and the lowermost  
515 stratosphere features a dynamic range of the backscatter signal of about eight decades, which means an extreme  
516 challenge for the detection electronics.

517 Based on continual improvements, starting with the 1994 system upgrading, the IFU ozone DIAL gradually  
518 approached a high performance until 2012, but minor potential for improvements remains. Comparison with the  
519 nearby mountain stations quite early demonstrated an uncertainty level of ±3 ppb in the lower troposphere.  
520 Occasional comparisons with ozone sondes launched at the Hohenpeißenberg (1996 to 2001, distance 38 km)  
521 were rather satisfactory up to the tropopause region.

522 Here, we analyse the lidar performance in three periods during its technical development in a more  
523 comprehensive manner. The best agreement was found for the side-by-side comparison with balloon ascents of  
524 ozone sondes, performed by the FZJ team at IMK-IFU in February 2019. Just a small, constant offset had to be

525 subtracted from the sonde data to achieve agreement. The lidar itself agreed with the three local summit stations.  
526 For all three years and all stations we determined a positive bias of just  $0.6 \text{ ppb} \pm 0.6 \text{ ppb}$ . This seems to reflect  
527 the -1.8-% calibration deficit of the WMO calibration of the in-situ ozone data. Thus, the lidar could be even free  
528 of bias in the lower free troposphere.

529 For the more distant MOHp sonde the comparisons are more demanding because of the high atmospheric  
530 variability (Vogelmann et al., 2011; 2015). This variability is particularly severe in summer when the  
531 atmospheric layering is more pronounced. Nevertheless, there was enough agreement in certain altitude ranges  
532 for examining the reliability of the ozone profiles obtained from the DIAL, also before the final modifications in  
533 2012. Between 2007 and 2011 we suspect an occasional slight negative summertime bias of the lidar of the order  
534 of 5 ppb above 6 km (not quantified because of insufficient data). This could be due to interfering structures on  
535 the 292-nm analogue signal (requiring mathematical correction) that could not be compensated by photon  
536 counting (available until 2003) and daylight-induced signal distortions at 313 nm (Trickl et al., 2020a). In  
537 principle, this calls for a re-evaluation of the ozone profiles for the wavelength pair 292 nm - 313 nm over the  
538 period 2007 to 2011, based on more recent experience in the signal inversion and the performance of the  
539 electronic equipment.

540 Vice versa, the lidar measurements helped us to validate the quality of the sonde measurements. Quite good  
541 agreement could be achieved by applying an altitude-independent offset correction to the ozone values that  
542 strongly varies from sonde to sonde. Most of the ozone differences the two sites are limited to altitudes below 2  
543 km. Thus, the differences reported earlier by Scheel for 3 km (see Introduction) are not caused by systematic  
544 differences in air composition at both sites. As can be seen from the figures presented in this paper the shifted  
545 sonde and the Zugspitze ozone mostly agrees to within  $\pm 3 \text{ ppb}$ . Given the frequently substantially higher ozone  
546 offsets of the MOHp sondes a recalibration of the archived sonde data based on comparisons with the Zugspitze  
547 or UFS in-situ data is advisable despite the considerable distance between the sites. Such a recalibration should  
548 be avoided in the presence of pronounced ozone structure around the station altitudes which could be accounted  
549 for by elevated uncertainties.

550 The comparisons for the three years 2000-2001, 2009 and 2018 reveal just minor performance change of the  
551 MOHp sonde over the years, with a variation of the annual average offset by about  $\pm 2 \text{ ppb}$ . We found a negative  
552 average offset of  $-3.64 \text{ ppb} \pm 3.72 \text{ ppb}$  (standard deviation) with respect to the IFU ozone DIAL over all three  
553 years. It is reasonable to assume that this offset is applicable to the entire tropospheric time series of the MOHp  
554 sondes.

555 Remaining tasks for the lidar are a substantial reduction of the solar background at 313.2 nm in summer and to  
556 enhance the moderate 291.8-nm backscatter signal in the upper troposphere. Further reduction of the residual  
557 solar background is difficult since the spectral filtering is already quite narrow. However, replacement of the  
558 rather aged (and partly contaminated) primary mirror of the far-field receiver could help by reducing the  
559 background radiation reflected into the detection system. As mentioned longer averaging is advisable. By longer  
560 averaging, the performance under low-aerosol conditions could almost reach that of in-situ measurements in a  
561 major part of the troposphere. Single-photon counting can also be helpful for longer averaging times, as  
562 demonstrated for our Raman lidar (Klanner et al., 2021). The noise level for counting is still lower than that of  
563 the meanwhile outstanding transient digitizers (Trickl et al., 2020a).

564  
565

566 **5 Data availability**

567 Lidar data and information on the lidar systems can be obtained on request from the IMK-IFU authors of this  
568 paper (thomas@trickl.de, hannes.vogelmann@kit.edu). The 313-nm aerosol backscatter coefficients are archived  
569 in the EARLINET data base, accessible through the ACTRIS data portal <http://actris.nilu.no/>. The  
570 Hohenpeißenberg ozone and humidity data are stored in the NDACC data archive ([https://www-  
571 air.larc.nasa.gov/missions/ndacc/data.html#](https://www-air.larc.nasa.gov/missions/ndacc/data.html#)). The data of the FIRMOS campaign is available via the ESA  
572 campaign dataset website <https://earth.esa.int/eogateway/campaigns/firmos>. The hourly Zugspitze and UFS  
573 ozone data are available at the World Data Center for Reactive Gases (WDCRG: <https://ebas.nilu.no/>) and the  
574 TOAR data base (Schultz et al., 2017).

575 **6 Author statement**

576 TT carried out most lidar measurements after spring 1997, following U. Kempfer and H. Eisele. He led the  
577 technical development of two ozone DIAL systems since 1990. HV was involved in the system upgrading since  
578 2007 and was responsible for the lidar operation during FIRMOS. DC and CW launched several ECC sondes at  
579 IMK-IFU in February 2019. MA and WS carried out the MOHp ozone sonde measurements. LR performed  
580 ozone in-situ measurements at UFS. MS provided LAGRANTO backward trajectories.

581 **7 Competing interests**

582 The authors declare that they have no conflict of interest.

583 **Acknowledgements**

584 The authors thank Wolfgang Seiler and Hans Peter Schmid for their support over so many years. The late Hans-  
585 Eckhart Scheel provided reference ozone data for the Wank, Zugspitze mountain stations in the vicinity of IMK-  
586 IFU. The different steps of lidar development have been funded by the German Ministry of Research and  
587 Technology (BMFT), the German Foundation for the Environment (DBU, two projects), and the Bavarian  
588 Ministry of Economics. Since 2007 the 313-nm aerosol results have contributed to EARLINET (European  
589 Aerosol Research Lidar Network) that is currently a part of the European Research Infrastructure ACTRIS  
590 (Aerosol, Clouds and Trace Gases Research Infrastructure). The lidar measurements were also funded by the  
591 European Union within Vertical Ozone Transport 1 and 2 (e.g., Wotava, G., and Kromp-Kolb, 2000; VOTALP  
592 2, 2000) and STACCATO (Stohl et al., 2003) and by the German Ministry for Research and Education (BMBF)  
593 within ATMOfAST (2005).

594 KIT acknowledges support of lidar measurements by the European Space Agency (ESA) under Contract  
595 4000123691/18/NL/NF (FIRMOS validation campaign). Balloon profiles utilized in this paper have been  
596 provided within the same ESA project by the Forschungszentrum Jülich via subcontract with KIT. The balloon  
597 activities were also partly supported by the Helmholtz Association in the framework of MOSES (Modular  
598 Observation Solutions for Earth Systems).

599 The service charges for this open access publication have been covered by a Research Centre of the Helmholtz  
600 Association.

601

602

603

604 **References**

- 605 ATMOFAST: Atmosphärischer Ferntransport und seine Auswirkungen auf die Spurengaskonzentrationen in der  
606 freien Troposphäre über Mitteleuropa (Atmospheric Long-range Transport and its Impact on the Trace-gas  
607 Composition of the Free Troposphere over Central Europe), Project Final Report, T. Trickl, co-ordinator, M.  
608 Kerschgens, A. Stohl, and T. Trickl, subproject co-ordinators, funded by the German Ministry of Education and  
609 Research within the programme “Atmosphärenforschung 2000“, <http://www.trickl.de/ATMOFAST.htm>, 130  
610 pp., 2005 (in German), with revised publication list of 2012
- 611 Ancellet, G., Pelon, J., Beekmann, M., Papayannis, A., and Mégie, G.: Ground-Based Lidar Studies of Ozone  
612 Exchanges Between the Stratosphere and the Troposphere, *J. Geophys. Res.*, 96, 22401-22421, 1991.
- 613 Ancellet, G., Godin-Beekmann, S., Smit, H. G. J., Stauffer, R. M., Van Malderen, R., Bodichon, R., and  
614 Pazmiño, A.: Homogenization of the Observatoire de Haute Provence electrochemical concentration cell (ECC)  
615 ozonesonde data record: comparison with lidar and satellite observations, *Atmos. Meas. Tech.*, 15, 3105–3120,  
616 2022.
- 617 Attmannspacher, W., and Dütsch, H.: 2nd International Ozone Sonde Intercomparison at the Observatory of  
618 Hohenpeissenberg, *Berichte des Deutschen Wetterdienstes* 157, 1981.
- 619 Beekmann, M., Ancellet, G., Mégie, G., Snit, H. G. J., and Kley, D.: Intercomparison Campaign of Vertical  
620 Ozone Profiles Including Electrochemical Sondes of ECC and Brewer-Mast Type and a Ground Based UV-  
621 Differential Absorption Lidar, *J. Atmos. Chem.*, 19, 259-288, 1994.
- 622 Belotti, C., Barbara, F., Barucci, M., Bianchini, G., D’Amato, F., Del Bianco, S., Di Natale, G., Gai, M.,  
623 Montori, A., Pratesi, F., Rolf, C., Sussmann, R., Trickl, T., Viciani, S., Vogelmann, H., Palchetti, L.: The Far-  
624 Infrared Radiation Mobile Observation System for spectral characterisation of the atmospheric emission, *Atmos.*  
625 *Meas. Tech.*, 16, 2511–2529, <https://doi.org/10.5194/amt-16-2511-2023>, 2023.
- 626 Brabec, M.: Backscatter and Humidity Measurements in Cirrus and Dust Clouds using Balloon Sondes, Ph.D.  
627 thesis, Eidgenössische Technische Hochschule, Zürich (Switzerland), 96 pp., 2011.
- 628 Brewer, A. W., and Milford, J. R.: The Oxford-Kew ozone sonde, *Proc. R. Soc. Lond. A*, 256, 470–495  
629 [available at <http://doi.org/10.1098/rspa.1960.0120>], 1960.
- 630 Browell, E. V., Danielsen, E. F., Ismail, S., Gregory, G. L., and Beck, S. M.: Tropopause Fold Structure  
631 Determined From Airborne Lidar and in Situ Measurements, *J. Geophys. Res.*, 92, 2112-2120, 1987.
- 632 Carnuth, W., and Trickl, T.: Transport studies with the IFU three-wavelength aerosol lidar during the VOTALP  
633 Mesolcina experiment, *Atmos. Environ.*, 34, 1425-1434, 2000.
- 634 Carnuth, W., Kempfer, U., and Trickl, T.: Highlights of the tropospheric lidar studies at IFU within the TOR  
635 project, *Tellus B*, 54, 163-185, 2002.
- 636 Claude, H., Hartmannsgruber, R., and Köhler, U.: Measurement of atmospheric profiles using the Brewer-Mast  
637 sonde, World Meteorological Organization, Global Ozone Res. and Monit. Proj. Report No. 17, WMO/TD No.  
638 179, Geneva (Switzerland), [see also [https://library.wmo.int/index.php?lvl=notice\\_display&id=11215](https://library.wmo.int/index.php?lvl=notice_display&id=11215)], 51 pp.,  
639 1987.



640 Deshler, T., Stübi, R., Schmidlin, F. J., Mercer, J. L., Smit, H. G. J., Johnson, B. J., Kivi, K., and Nardi, B.:  
641 Methods to homogenize electrochemical concentration cell (ECC) ozonesonde measurements across changes in  
642 sensing solution concentration or ozonesonde manufacturer, *Atmos. Meas. Tech.*, 10, 2021–2043, 2017.

643 Daumont, D., Brion, J., Charbonnier, J., and Malicet, J.: Ozone UV Spectroscopy I: Absorption Cross-Sections  
644 at Room Temperature, *J. Atmos. Chem.*, 15, 145-155, 1992.

645 Davies, W. E., Vaughan, G., and O'Connor, F. M.: Observation of near-zero ozone concentrations in the upper  
646 troposphere at mid-latitudes, *Geophys. Res. Lett.*, 25, 1173-1176, 1998.

647 De Backer, H., De Muer, D., and De Sadelaer G.: Comparison of ozone profiles obtained with Brewer-Mast and  
648 Z-ECC sensors during simultaneous ascents, *J. Geophys. Res.*, 103, 19,641–19,648,  
649 <https://doi.org/10.1029/98JD01711>, 1998.

650 De Muer, D., and Malcorps, H.: The frequency response of an electrochemical ozone sonde and its application to  
651 the deconvolution of ozone profiles, *J. Geophys. Res.*, 89, 1361–1372, 1984.

652 Di Natale, G., Barucci, M., Belotti, C., Bianchini, G., D'Amato, F., Del Bianco, S. Gai, M., Montori, A.,  
653 Sussmann, R., Viciani, S., Vogelmann, H., and Palchetti, L.: Comparison of mid-latitude single- and mixed-  
654 phase cloud optical depth from co-located infrared spectrometer and backscatter lidar measurements, *Atmos.*  
655 *Meas. Tech.*, 14, 6749–6758, 2021.

656 Dirksen, R. J., Sommer, M., Immler, F. J., Hurst, D. F., Kivi, R., and Vömel, H.: Reference quality upper-air  
657 measurements: GRUAN data processing for the Vaisala RS92 radiosonde, *Atmos. Meas. Tech.*, 7, 4463-4490,  
658 [doi.org/10.5194/amt-7-4463-2014](https://doi.org/10.5194/amt-7-4463-2014), 2014.

659 Draxler, R., and Hess, G.: An overview of the HYSPLIT\_4 modelling system for trajectories, dispersion, and  
660 deposition, *Aust. Meteorol. Mag.*, 47, pp. 295-308, 1998.

661 Eisele, H., Trickl, T., and Claude, H.: Lidar als wichtige Ergänzung zur Messung troposphärischen Ozons,  
662 *Ozonbulletin des Deutschen Wetterdiensts*, 44, 2 pp., 1997 (in German).

663 Eisele, H., Scheel, H. E., Sladkovic, R., and Trickl, T.: High-Resolution Lidar Measurements of Stratosphere-  
664 Troposphere Exchange, *J. Atmos. Sci.*, 56, 319-330, 1999.

665 Eisele, H., and Trickl, T.: Improvements of the aerosol algorithm in ozone-lidar data processing by use of  
666 evolutionary strategies, *Appl. Opt.*, 44, 2638-2651, 2005.

667 EUROTRAC: Transport and Chemical Transformation of Pollutants in the Troposphere, Vol. 1, An Overview of  
668 the Work of EUROTRAC, P. Borrell and P. M. Borrell, Eds., Springer (Berlin, Heidelberg, New York), ISBN 3-  
669 540-66775-X, 474 pp., 1997.

670 Gaudel, A., Ancellet G., and Godin-Beekmann S.: Analysis of 20 years of tropospheric ozone vertical profiles by  
671 lidar and ECC at Observatoire de Haute Provence (OHP) at 44° N, 6.7° E, *Atmos. Environ.*, 113, 78-89, 2015.

672 Gaudel, A., Cooper, O. R., Ancellet, G., Barret, B., Boynard, A., Burrows, J. P., Clerbaux, J. P., Coheur, P.-F.,  
673 Cuesta, J., Cuevas, E., Doniki, S., Dufour, G., Ebojic, F., Foret, G., Garcia, O., Granados-Muñoz, M. J.,  
674 Hannigan, J., Hase, F., Hassler, B., Huang, G., Hurtmans, D., Jaffe, D., Jones, N., Kalabokas, P., Kerridge, B.,  
675 Kulawik, S., Latter, B., Leblanc, T., Le Flochmoën, E., Lin, W., Liu, J., Liu, X., Mahieu, E., McClure-Begley,  
676 A., Neu, J., Osman, M., Palm, M., Petetin, H., Petropavlovskikh, I., Querel, R., Rappoe, N., Rozanov, A.,  
677 Schultz, M. G., Schwab, J., Siddans, R., Smale, D., Steinbacher, M., Tanimoto, H., Tarasick, D., Thouret, V.,

678 Thompson, A., M., Trickl, T., Weatherhead, E., Wespes, C., Worden, H., Vigouroux, C., Xu, X., Zeng, G.,  
679 Ziemke, J.: Tropospheric Ozone Assessment Report: Present-day distribution and trends of tropospheric ozone  
680 relevant to climate and global atmospheric chemistry model evaluation, *Elem. Sci. Anth.*, 6, 39, DOI:  
681 [https://doi.org/ 10.1525/elementa.291](https://doi.org/10.1525/elementa.291), 58 pp., 2018.

682 Grant, W. B., Browell, E. V., Butler, C. F., Fenn, M. A., Clayton, M. B., Hannan, J. R., Fuelberg, H. E., Blake,  
683 D. R., Blake, N. J., Gregory, G. L., Heikes, B. G., Sachse, G. W., Singh, H. B., Snow, J., and Talbot, R. W.: A  
684 case study of transport of tropical marine boundary layer and lower tropospheric air masses to the northern  
685 midlatitude upper troposphere, *J. Geophys. Res.*, 105, 3757-3769, 2000.

686 Hearn, A. G.: The Absorption of Ozone in the Ultra-violet and Visible Regions of the Spectrum, *Proc. Phys.*  
687 *Soc.*, 78, 932-940, 1961.

688 Hersbach, H., Bell, B., Berrisford, P., Simmons, A., Berrisford, P., Dahlgren, P., Horanyi, A., Muñoz-Sabater, J.,  
689 Nicolas, J., Radu, R., Schepers, D., Soci, C., Villaume, S., Bidlot, J. R., Haimberger, L.; Woollen, J.,  
690 Buontempo, C., and Thepaut, J. N.: The ERA5 global reanalysis. *Q. J. R. Meteorol Soc.*, 146, 1999– 2049,  
691 <https://doi.org/10.1002/qj.3803>, 2020.

692 Johnson, B. J., Oltmans, S. J., Vömel, H., Smit, H. G. J., Deshler, T., and Kröger, C.: Electrochemical  
693 concentration cell (ECC) ozonesonde pump efficiency measurements and tests on the sensitivity to ozone of  
694 buffered and unbuffered ECC sensor cathode solutions, *J. Geophys. Res.-Atmos.*, 107, ACH 8-1–ACH 8-18,  
695 <https://doi.org/10.1029/2001JD000557>, 2002.

696 Jeannot, P., Stübi, R., Levrat, G., Viatte, P., and J. Staehelin, J.: Ozone balloon soundings at Payerne  
697 (Switzerland): Reevaluation of the time series 1967–2002 and trend analysis, *J. Geophys. Res.*, 112, D11302,  
698 doi:10.1029/2005JD006862, 15 pp., 2007.

699 Kempfer, U., Carnuth, W., Lotz, R., and Trickl, T.: A wide range ultraviolet lidar system for tropospheric ozone  
700 measurements: development and application, *Rev. Sci. Instrum.*, 65, 3145-3164, 1994.

701 Kerr, J. B., Fast, H., McElroy, C.T., Oltmans, S.J., Lathrop, J.A., Kyro, E., Paukkunen, A., Claude, H., Köhler,  
702 U., Sreedharan, C.R., akao T., and Tsukagoshi, Y.: The 1991 WMO International Ozonesonde Intercomparison  
703 at Vanskoy, Canada. *Atmos.–Ocean*, 32, 685–716, <https://doi.org/10.1080/07055900.1994.9649518>, 1994.

704 Klanner, L., Höveler, K., Khordakova, D., Perfahl, M., Rolf, C., Trickl, T., and Vogelmann, H.: A powerful lidar  
705 system capable of 1 h measurements of water vapour in the troposphere and the lower stratosphere as well as the  
706 temperature in the upper stratosphere and mesosphere, *Atmos. Meas. Tech.*, 14, 531-555, 2021.

707 Klausen, J., Zellweger, C., Buchmann, B., and Hofer, P.: Uncertainty and bias of surface ozone measurements at  
708 selected Global Atmospheric Watch sites, *J. Geophys. Res.*, 108, 4622, doi: 10.1029/2003JD003710, 17 pp.,  
709 2003.

710 Kley, D., Beck, J., Grennfelt, P. I., Hov, O., and Penkett, S. A.: Tropospheric Ozone Research (TOR) A Sub-  
711 Project of EUROTRAC, *J. Atmos. Chem.*, 28, 1–9, 1997.

712 Kley, D., Crutzen, P. J., Smit, H. G. J., Vömel, H., Oltmans, S., Grassl, H., and Ramanathan, V.: Observations of  
713 Near-Zero Ozone Concentrations Over the Convective Pacific: Effects on Air Chemistry, *Science*, 274, 230-233,  
714 1996.

715 Komhyr, W.D.: Electrochemical concentration cells for gas analysis, *Ann. Geoph.*, 25, 203–210, 1969.

716 Komhyr, W. D., Barnes, R. A., Brothers, G. B., Lathrop, J. A., and Opperman, D. P.: Electrochemical  
717 concentration cell ozonesonde performance evaluation during STOIC 1989, *J. Geophys. Res.*, 100, 9231–9244,  
718 <https://doi.org/10.1029/94JD02175>, 1995.

719 Langford, A. O., Masters, C. D., Proffitt, M. H., Hsie, E.-Y., and Tuck, A. F.: Ozone measurements in a  
720 tropopause fold associated with a cut-off low system, *Geophys. Res. Lett.*, 23, 2501–2504, 1996.

721 Logan, J.A., Staehelin, J., Megretskaja, I.A., Cammas, J.-P., Thouret, V., Claude, H., De Backer, H.,  
722 Steinbacher, M., Scheel, H.-E., Stübi, R., Fröhlich, M., and Derwent, R. (2012), Changes in ozone over Europe:  
723 Analysis of ozone measurements from sondes, regular aircraft (MOZAIC) and alpine surface sites, *J. Geophys.*  
724 *Res.*, 117, D09301, doi:10.1029/2011JD016952.

725 Malicet, J., Daumont, D., Charbonnier, J., Parisse, C., Chakir, A., and Brion, J.: Ozone UV Spectroscopy I:  
726 Absorption Cross-Sections and Temperature Dependence, *J. Atmos. Chem.*, 21, 263-273, 1995.

727 Palchetti, L., Barucci, M., Belotti, C., Bianchini, G., Cluzet, B., D'Amato, F., Del Bianco, S., Di Natale, G., Gai,  
728 M., Khordakova, D., Montori, A., Oetjen, H., Rettinger, M., Rolf, C., Schuettemeyer, D., Sussmann, R., Viciani,  
729 S., Vogelmann, H., and Wienhold, F. G.: Observations of the downwelling far-infrared atmospheric emission at  
730 the Zugspitze observatory, *Earth Syst. Sci. Data*, 13, 4303–4312, <https://doi.org/10.5194/essd-13-4303-2021>,  
731 2021.

732 Parrish, D. D., Derwent, R. G., Steinbrecht, W., Stübi, R., Van Malderen, R., Steinbacher, M., Trickl, T., Ries,  
733 L., and Xu, X.: Zonal Similarity of Long-term Changes and Seasonal Cycles of Baseline Ozone at Northern  
734 Mid-latitudes, *J. Geophys. Res.*, 125, e2019JD031908, <https://doi.org/10.1029/2019JD031908>, 19 pp., 2020.

735 Schultz, M. G., Schröder, S., Lyapina, O., Cooper, O., Galbally, I., Petropavlovskikh, I., von Schneidmesser,  
736 E., Tanimoto, H., Elshorbany, Y., Naja, M., Seguel, R. J., Dauert, U., Eckhardt, P., Feigenspan, S., Fiebig, M.,  
737 Hjellbrekke, A.-G., Hong, Y.-D., Kjeld, P. C., Koide, H., Lear, G., Tarasick, D., Ueno, M., Wallasch, M.,  
738 Baumgardner, D., Chuang, M.-T., Gillett, R., Lee, M., Molloy, S., Moolla, R., Wang, T., Sharps, K., Adame, J.  
739 A., Ancellet, G., Apadula, F., Artaxo, P., Barlasina, M. E., Bogucka, M., Bonasoni, P., Chang, L., Colomb, A.,  
740 Cuevas-Agulló, E., Cupeiro, M., Degorska, A., Ding, A., Fröhlich, M., Frolova, M., Gadhavi, H., Gheusi, F.,  
741 Gilge, S., Gonzalez, M. Y., Gros, V., Hamad, S. H., Helmig, D., Henriques, D., Hermansen, O., Holla, R.,  
742 Hueber, J., Im, U., Jaffé, D. A., Komala, N., Kubistin, D., Lam, K.-S., Laurila, T., Lee, H., Levy, I., Mazzoleni,  
743 C., Mazzoleni, L. R., McClure-Begley, A., Mohamad, M., Murovec, M., Navarro-Comas, M., Nicodim, F.,  
744 Parrish, D., Read, K. A., Reid, N., Ries, L., Saxena, P., Schwab, J. J., Scorgie, Y., Senik, I., Simmonds, P.,  
745 Sinha, V., Skorokhod, A. I., Spain, G., Spangl, W., Spoor, R., Springston, S. R., Steer, K., Steinbacher, M.,  
746 Suharguniyawan, E., Torre, P., Trickl, T., Weili, L., Weller, R., Xiaobin, X., Xue, L., and Zhiqiang, M.:  
747 Tropospheric Ozone Assessment Report: Database and Metrics Data of Global Surface Ozone Observations,  
748 *Elem. Sci. Anth.*, 5, 58, DOI: <https://doi.org/10.1525/elementa.244>, 25 pp., 2017.

749 Reichardt, J., Ansmann, A., Serwazi, M., Weitkamp, C., and Michaelis, W.: Unexpectedly low ozone  
750 concentration in midlatitude tropospheric ice clouds: A case study, *Geophys. Res.Lett.*, 23, 1929-1932, 1996.

751 Smit, H. G. J, Straeter, W., Johnson, B. J., Oltmans, S. J., Davies, J., Tarasick, D. W., Hoegger, B., Stubi, R.,  
752 Schmidlin, F. J., Northam, T., Thompson, A. M., Witte, J. C., Boyd, I., and Posny, F.: Assessment of the  
753 Performance of ECC-ozonesondes under Quasi-flight Conditions in the Environmental Simulation Chamber:  
754 Insights from the Jülich Ozone Sonde Intercomparison Experiment (JOSIE), *J. Geophys. Res.*, 112, D19306,  
755 doi:10.1029/2006JD007308, 18 pp., 2007.

756 Smit, H.G.J., and ASOPOS panel: Quality assurance and quality control for ozonesonde measurements in GAW,  
757 World Meteorological Organization, GAW Report No. 201, Geneva (Switzerland). [Available online at  
758 [https://library.wmo.int/doc\\_num.php?explnum\\_id=7167](https://library.wmo.int/doc_num.php?explnum_id=7167)], 100 pp., 2014.

759 Smit, H.G.J., and Thompson, A.M.: Ozonesonde Measurement Principles and Best Operational Practices:  
760 ASOPOS 2.0 (Assessment of Standard Operating Procedures for Ozonesondes), World Meteorological  
761 Organization, GAW Report No. 268, Geneva (Switzerland). [Available online at  
762 [https://library.wmo.int/doc\\_num.php?explnum\\_id=10884](https://library.wmo.int/doc_num.php?explnum_id=10884)], 172 pp., 2021.

763 Stauffer, R.M., Thompson, A.M., Kollonige, D.E., Tarasick, D.W., Van Malderen, R., Smit, H.G.J., Vömel, H.,  
764 Morris, G.A., Johnson, B.J., Cullis, P.D., Stübi, R., Davies, J., and Yan.: An Examination of the Recent Stability  
765 of Ozonesonde Global Network Data, *Earth and Space Science*, 9 (10), e2022EA002459, [available online at  
766 <https://doi.org/10.1029/2022EA002459>], 2022.

767 Stein, A. F., Draxler, R. R., Rolph, G. D., Stunder, B. J. B., Cohen, M. D., and Ngan, F.: NOAA's HYSPLIT  
768 atmospheric transport and dispersion modeling system, *Bull. Amer. Meteor. Soc.*, 96, 2059-2077, 2015.

769 Steinbrecht, W., Schwarz, R., and Claude, H.: New pump correction for the Brewer-Mast ozone sonde:  
770 determination from experiment and instrument intercomparisons, *J. Atmos. Ocean. Tech.*, 15, 144–156, 1998.

771 Stohl, A., and Trickl, T.: A textbook example of long-range transport: Simultaneous observation of ozone  
772 maxima of stratospheric and North American origin in the free troposphere over Europe, *J. Geophys. Res.*, 104,  
773 30445-30462, 1999.

774 Stohl, A., Bonasoni, P., Cristofanelli, P., Collins, W., Feichter, J., Frank, A., Forster, C., Gerasopoulos, E.,  
775 Gäggeler, H., James, P., Kentarchos, T., Kromp-Kolb, H., Krüger, B., Land, C., Meloan, J., Papayannis, A.,  
776 Priller, A., Seibert, P., Sprenger, M., Roelofs, G. J., Scheel, H. E., Schnabel, C., Siegmund, P., Tobler, L., Trickl,  
777 T., Wernli, H., Wirth, V., Zanis, P., and Zerefos, C.: Stratosphere-troposphere exchange - a review, and what we  
778 have learned from STACCATO, *J. Geophys. Res.*, 108, 8516, doi:10.1029/2002JD002490, STA 1, 15 pp., 2003.

779 Stübi, R., Levrat, G., Hoegger, B., Pierre Viatte, P., Staehelin, J., Schmidlin, F.J.: In-flight comparison of  
780 Brewer-Mast and electrochemical concentration cell ozonesondes, *J. Geophys. Res.*, 113, D13302,  
781 <https://doi.org/10.1029/2007JD009091>, 2008.

782 Tarasick, D. W., Davies, J., Anlauf, K., Watt, M., Steinbrecht, W., Claude H.-J.: Laboratory investigations of the  
783 response of Brewer-Mast ozonesondes to tropospheric ozone, *J. Geophys. Res.*, 107, ACH 14-1 – 14-10,  
784 <https://doi.org/10.1029/2001JD001167>, 2002.

785 Tarasick, D. W., Davies, J., Smit, H. G. J., and Oltmans, S. J.: A re-evaluated Canadian ozonesonde record:  
786 measurements of the vertical distribution of ozone over Canada from 1966 to 2013, *Atmos. Meas. Tech.*, 9, 195–  
787 214, <https://doi.org/10.5194/amt-9-195-2016>, 2016.

788 Tarasick, D., Galbally, I. E., Cooper, O. R., Schultz, G M., Ancellet, G., Leblanc, T., Wallington, T. J., Ziemke,  
789 J., Liu, X., Steinbacher, M., Staehelin, J., Vigouroux, C., Hannigan, J., García, O., Foret, G., Zanis, P.,  
790 Weatherhead, E., Petropavlovskikh, I., Worden, H., Osman, M., Liu, J., Chang, K.-L., Gaudel, A., Lin, M.,  
791 Granados-Muñoz, M., Thompson, A. M., Oltmans, S. J., Cuesta, J., Dufour, G., Thouret, V., Hassler, B., Trickl,  
792 T., and Neu, J. L.: Tropospheric Ozone Assessment Report: Tropospheric ozone from 1877 to 2016, observed  
793 levels, trends and uncertainties, *Elem. Sci. Anth.*, 7, Article 39, DOI: <https://doi.org/10.1525/elementa.376>, 72  
794 pp. (plus 56 pp. of supplemental material), 2019.

795 Tarasick, D. W., Smit, H. G. J., Thompson, A. M., Morris, G. A., Witte, J. C., Davies, J., Davies, J., Nakano, T.,  
796 Van Malderen, R., Stauffer, R. M., Johnson, B. J., Stubi1, R., Oltmans, S. J., and Vömel, H.: Improving ECC  
797 ozonesonde data quality: Assessment of current methods and outstanding issues, *Earth and Space Science*, 8,  
798 e2019EA000914. <https://doi.org/10.1029/2019EA000914>, 27 pp., 2021.

799 TESLAS: Tropospheric Environmental Studies by Laser Sounding (TESLAS), in: *Transport and Chemical*  
800 *Transformation of Pollutants in the Troposphere*, Vol. 8, Instrument Development for Atmospheric Research and  
801 Monitoring, J. Bösenberg, D. Brassington, and P. C. Simon, Eds., Springer (Berlin, Heidelberg, New York),  
802 ISBN 3-540-62516-X, 1-203, 1997.

803 Thompson, A. M., Smit, H. G. J., Witte, J. C., Stauffer, R. M., Johnson, B. J., Morris, G., von der Gathen, P.,  
804 Van Malderen, R., Davies, J., Piters, A., Allaart, M., Posny, F., Kivi, R., Cullis, P., Hoang Anh, N. T., Corrales,  
805 E., Machinini, T., da Silva, F. R., Paiman, G., Thiong'o, K., Zainal, Z., Brothers, G. B., Wolff, K. R., Nakano,  
806 T., Stübi, R., Romanens, G., Coetzee, G. J. R., Diaz, J. A., Mitro, S., Mohamad, M., and Ogino, S.: Ozonesonde  
807 Quality Assurance: The JOSIE–SHADOZ (2017) Experience, *Bulletin of the American Meteorological Society*,  
808 100, 155-171, 2019.

809 Trickl, T., Cooper, O. R., Eisele, H., James, P., Mücke, R., and Stohl, A.: Intercontinental transport and its  
810 influence on the ozone concentrations over central Europe: Three case studies, *J. Geophys. Res.*, 108, D12, 8530,  
811 10.1029/2002JD002735, *STA* 15, 23 pp., 2003.

812 Trickl, T., Feldmann, H., Kanter, H.-J., Scheel, H. E., Sprenger, M., Stohl, A., and Wernli, H.: Deep  
813 stratospheric intrusions over Central Europe: case studies and climatological aspects, *Atmos. Chem. Phys.*, 10,  
814 499-524, 2010.

815 Trickl, T., Eisele, H., Bärtsch-Ritter, N., Furger, M., Mücke, R., Sprenger, M., and Stohl, A.: High-ozone layers  
816 in the middle and upper troposphere above Central Europe: potential import from the stratosphere along the  
817 subtropical jet stream, *Atmos. Chem. Phys.*, 11, 9343-9366; 5-p. Supplement, 2011.

818 Trickl, T., Vogelmann, H., Giehl, H., Scheel, H. E., Sprenger, M., and Stohl, A.: How stratospheric are deep  
819 stratospheric intrusions? *Atmos. Chem. Phys.*, 14, 9941-9961, 2014.

820 Trickl, T., Vogelmann, H., Flentje, H., and Ries, L.: Stratospheric ozone in boreal fire plumes – the 2013 smoke  
821 season over Central Europe, *Atmos. Chem. Phys.*, 15, 9631-9649, 2015.

822 Trickl, T., Vogelmann, H., Fix, A., Schäfler, A., Wirth, M., Calpini, B., Levrat, G., Romanens, G., Apituley, A.,  
823 Wilson, K. M., Begbie, R., Reichardt, J., Vömel, H. and Sprenger, M.: How stratospheric are deep stratospheric  
824 intrusions into the troposphere? LUAMI 2008, *Atmos. Chem. Phys.*, 16, 8791-8815, 2016.

825 Trickl, T., Neidl, F., Giehl, H., Perfahl, M., and Vogelmann, H.: Three decades of tropospheric ozone lidar  
826 development at Garmisch-Partenkirchen, *Atmos. Meas. Tech.*, 13, 6357-6390, 2020a.

827 Trickl, T., Vogelmann, H., Ries, L., and Sprenger, M.: Very high stratospheric influence observed in the free  
828 troposphere over the Northern Alps – just a local phenomenon? *Atmos. Chem. Phys.*, 20, 243-266, 2020b.

829 Trickl, T., Couret, C., Ries, L., and Vogelmann, H.: Zugspitze ozone 1978 – 2020: The role of stratosphere-  
830 troposphere transport, *Atmos. Chem. Phys.*, ACP-2022-783, under final review (2023)

831 Vaisala: Vaisala Radiosonde RS41 Measurement Performance, White Paper, Vaisala, Helsinki (Finland),  
832 [https://www.vaisala.com/sites/default/files/documents/WEA-MET-RS41-Performance-White-paper-](https://www.vaisala.com/sites/default/files/documents/WEA-MET-RS41-Performance-White-paper-B211356EN-B-LOW-v3.pdf)  
833 [B211356EN-B-LOW-v3.pdf](https://www.vaisala.com/sites/default/files/documents/WEA-MET-RS41-Performance-White-paper-B211356EN-B-LOW-v3.pdf), 28 pp. (accessed 7 September 2019), 2017.

834 Van Malderen, R., Allaart, M. A. F., De Backer, H., Smit, H. G. J., and De Muer, D.: On instrumental errors and  
835 related correction strategies of ozonesondes: possible effect on calculated ozone trends for the nearby sites Uccle  
836 and De Bilt, *Atmos. Meas. Tech.*, 9, 3793–3816, 2016

837 Viallon, J., Lee, S., Moussay, P., Tworek, K., Peterson, M., and Wielgosz, R. I.: Accurate measurements of  
838 ozone absorption cross-sections in the Hartley band, *Atmos. Meas. Tech.*, 8, 1245-1257, 2015.

839 Völger, P., Bösenberg, J., and Schult, I.: Scattering Properties of Selected Model Aerosols Calculated at UV-  
840 Wavelengths: Implications for DIAL Measurements of Tropospheric Ozone, *Beitr. Phys. Atmosph.*, 69, 177-  
841 187, 1996.

842 Vömel, H., David, D. E., and Smith, K.: Accuracy of tropospheric and stratospheric water vapor measurements  
843 by the cryogenic frost point hygrometer: Instrumental details and observations, *J. Geophys. Res.*, 112, D08305,  
844 doi: 10.1029/2006JD007224, 14 pp., 2007.

845 Vömel, H., Naebert, T., Dirksen, R., and Sommer, M.: An update on the uncertainties of water vapor  
846 measurements using Cryogenic Frostpoint Hygrometers, *Atmos. Meas. Tech.*, 9, 3755-3768, 2016.

847 Vömel, H., Smit, H. G. J., Tarasick, D., Johnson, B., Oltmans, S. J., Selkirk, H., Thompson, A. M., Stauffer, R.  
848 M., Witte, J. C., Davies, J., van Malderen, R., Morris, G. A., Nakano, T., and Stübi, R.: A new method to correct  
849 the electrochemical concentration cell (ECC) ozonesonde time response and its implications for “background  
850 current” and pump efficiency, *Atmos. Meas. Tech.*, 13, 5667–5680, 2020.

851 Vogelmann, H. and Trickl, T.: Wide-Range Sounding of Free-Tropospheric Water Vapor with a Differential-  
852 Absorption Lidar (DIAL) at a High-Altitude Station, *Appl. Opt.*, 47, 2116-2132, 2008.

853 Vogelmann, H., Sussmann, R., Trickl, T., and Borsdorff, T.: Intercomparison of atmospheric water vapor  
854 soundings from the differential absorption lidar (DIAL) and the solar FTIR system on Mt. Zugspitze, *Atmos.*  
855 *Meas. Tech.*, 4, 835-841, 2011.

856 Vogelmann, H., Sussmann, R., Trickl, T., and Reichardt, A.: Spatiotemporal variability of water vapor  
857 investigated using lidar and FTIR vertical soundings above the Zugspitze, *Atmos. Chem. Phys.*, 14, 3135-3148,  
858 2015.

859 VOTALP II: Vertical Ozone Transport in the Alps II, Final Report for the European Union, Contract Nr.: ENV4  
860 CT970413, Reporting Period 1/3/1998-29/2/2000, H. Kromp-Kolb, Co-ordinator, Universität für Bodenkultur  
861 Wien (Austria), Institut für Meteorologie und Physik, 96 pp., 2000.

862 Wernli, H., and Davies, H.C.: A Lagrangian-based analysis of extratropical cyclones. I: The method and some  
863 applications. *Q.J.R. Meteorol. Soc.*, 123: 467-489, <https://doi.org/10.1002/qj.49712353811>, 1997.

864 Sprenger, M., and Wernli, H.: The LAGRANTO Lagrangian analysis tool – version 2.0, *Geosci. Model Dev.*, 8,  
865 2569–2586, <https://doi.org/10.5194/gmd-8-2569-2015>, 2015.

866 Wotava, G., and Kromp-Kolb, H.: The research project VOTALP – general objectives and main results, *Atmos.*  
867 *Environ.*, 34, 1319-1322, 2000.

868 Yuan, Y., Ries, L., Petermeier, H., Trickl, T., Leuchner, M., Couret, C., Sohmer, R., Meinhardt, F., and Menzel,  
869 A.: On the diurnal, weekly, and seasonal cycles and annual trends in atmospheric CO<sub>2</sub> at Mount Zugspitze,  
870 Germany, during 1981–2016, *Atmos. Chem. Phys.*, 19, 999–1012, <https://doi.org/10.5194/acp-19-999-2019>,  
871 2019.

872 Zanis, P., Trickl, T., Stohl, A., Wernli, H., Cooper, O., Zerefos, C., Gaeggeler, H., Priller, A., Schnabel, C.,  
873 Scheel, H. E., Kanter, H. J., Tobler, L., Kubik, P. W., Cristofanelli, P., Forster, C., James, P., Gerasopoulos, E.,  
874 Delcloo, A., Papayannis, A., and Claude, H.: Forecast, observation and modelling of a deep stratospheric  
875 intrusion event over Europe, *Atmos. Chem. Phys.*, 3, 763-777, 2003.

876 Zellweger, C., Buchmann, B., Klausen, J., and Hofer, P.: System and Performance Audit of Surface Ozone,  
877 Carbon Monoxide and Methane at the Global GAW Station Zugspitze/Hohenpeißenberg, Platform Zugspitze,  
878 Germany, Empa-WCC Report 01/1, submitted to the World Meteorological Organization, 49 pp., February  
879 2001.

880 Zellweger, C., Klausen, J., and Buchmann, B.: System and Performance Audit of Surface Ozone, Carbon  
881 Monoxide and Methane at the Global GAW Station Zugspitze/Schneefernerhaus, Germany, Empa-WCC Report  
882 06/2, submitted to the World Meteorological Organization, 51 pp., June 2006.

883 Zellweger, C., Steinbacher, M., and Buchmann, B., and Steinbrecher, R.: System and Performance Audit of  
884 Surface Ozone, Methane, Carbon Dioxide, Nitrous Oxide and Carbon Monoxide at the Global GAW Station  
885 Zugspitze-Schneefernerhaus, Germany, submitted to WMO by WMO World Calibration Centre WCC-Empa  
886 Empa Dübendorf, Switzerland, 46. pp., WCC-Empa Report 11/2, June 2011.

887 Zellweger, C., Steinbacher, M., Buchmann, B., and Steinbrecher, R.: System and Performance Audit of Surface  
888 Ozone, Methane, Carbon Dioxide, Nitrous Oxide and Carbon Monoxide at the Global GAW Station Zugspitze-  
889 Schneefernerhaus, Germany, submitted to WMO by WMO World Calibration Centre WCC-Empa Empa  
890 Dübendorf, Switzerland, WCC-Empa Report 20/3, September 2020, GAW report 266, 54. pp., 2021.

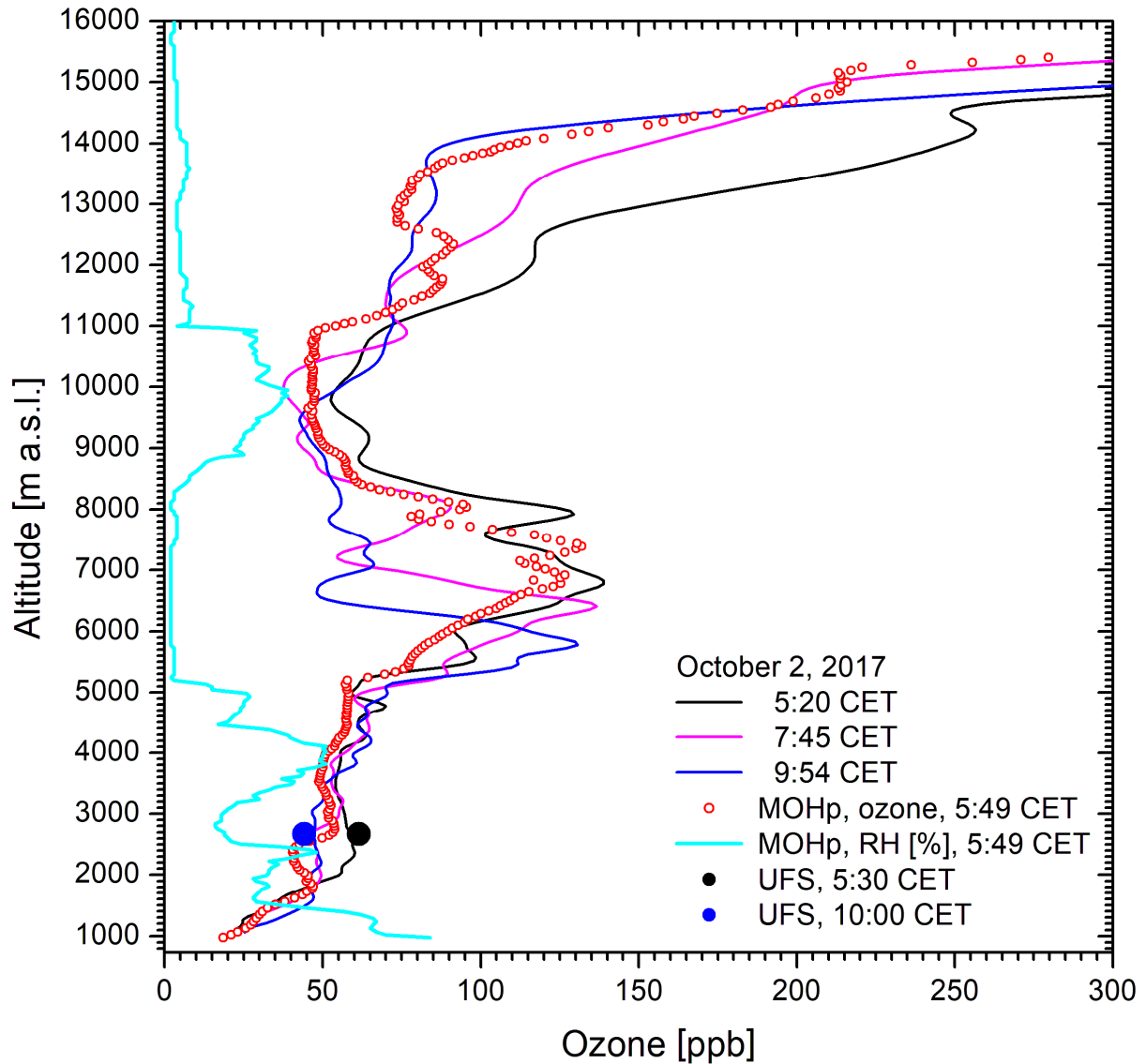
891

892

893 Figures:

894

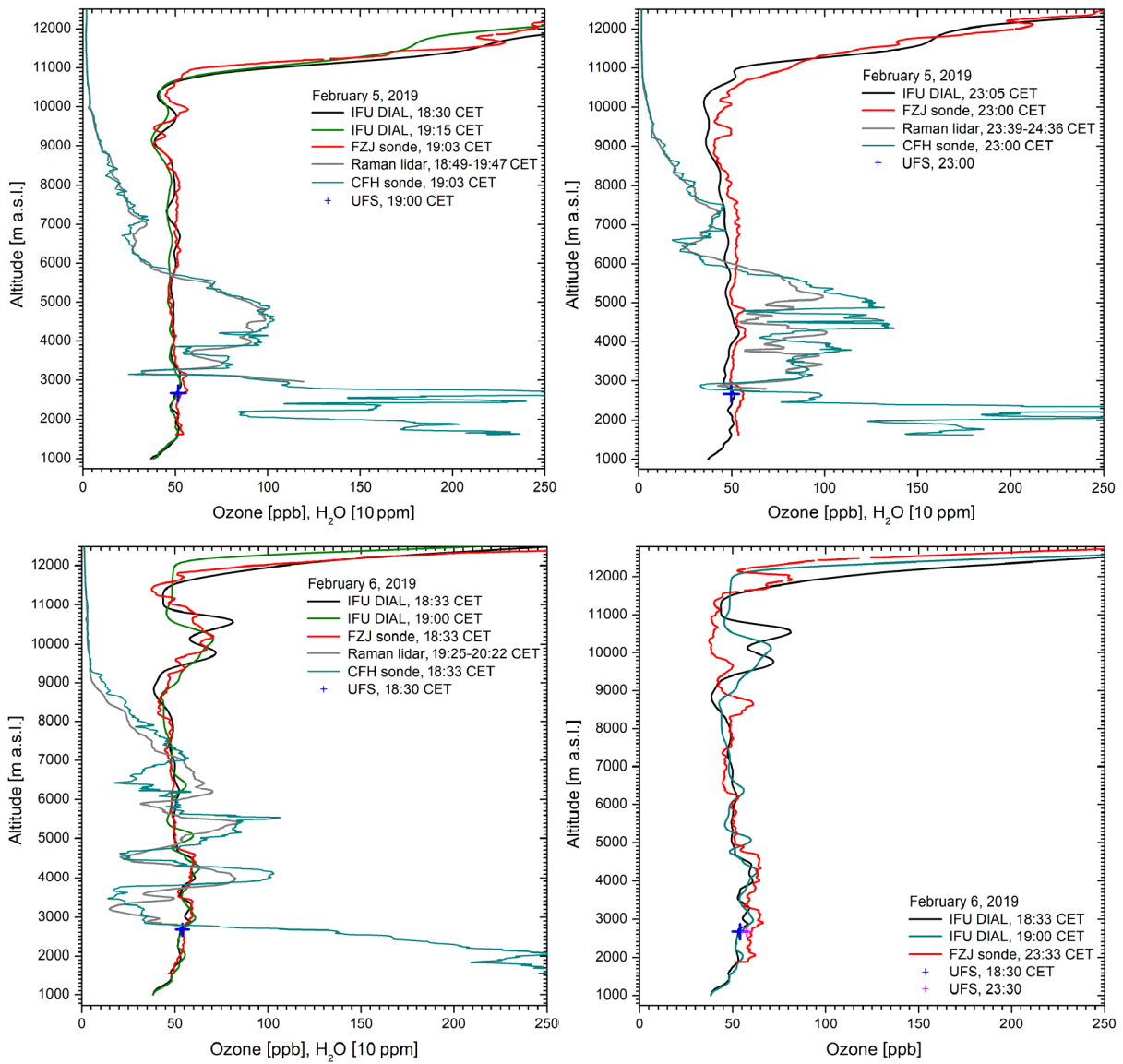
895



896 **Fig. 1.** Ozone measurements at Garmisch-Partenkirchen (IFU, UFS) and Hohenpeißenberg (MOHp) on 2  
897 October 2017; the low relative humidity between 5.2 and 8.3 km (RH = 2 %) verifies the presence of a  
898 stratospheric air intrusion. The time for MOHp is the launch time of the sonde.

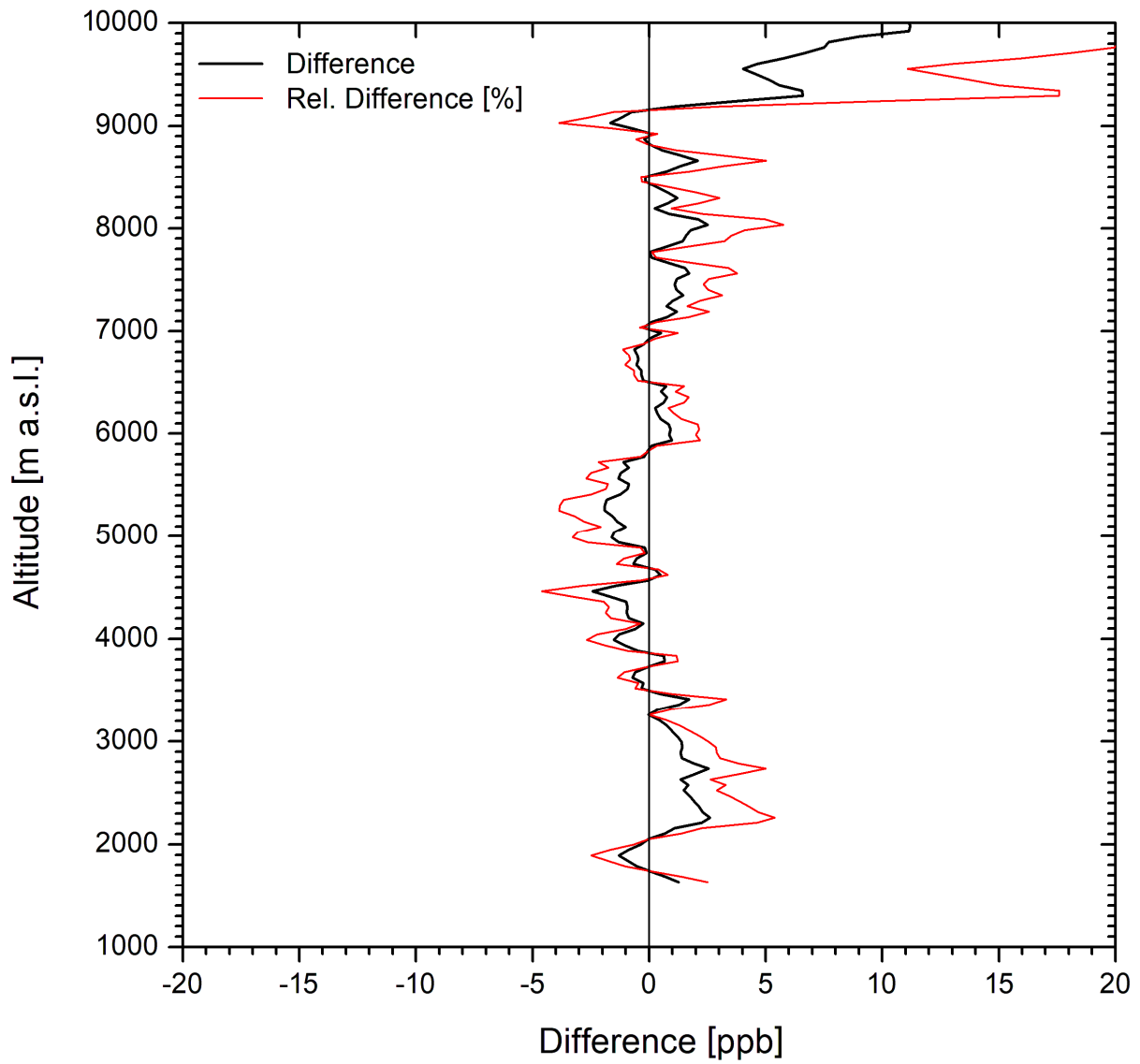
899





901 **Fig. 2.** Four ozone measurements on 5 and 6 February 2019 with lidar (IFU), ECC sonde (FZJ) and an in-situ  
 902 sensor at UFS; for two measurements the FZJ ozone mixing ratios are slightly higher than the lidar results. The  
 903 fourth FZJ ozone measurement took place much later than the final lidar measurements which resulted in slightly  
 904 larger differences. The lidar results around 10 km on 6 February are uncertain due to a cirrus correction. In order  
 905 to visualize more details on the complex layering we also show water-vapour mixing ratios for roughly co-  
 906 inciding measurements of the UFS Raman lidar and the FZJ CFH sonde. The tropospheric structures are strongly  
 907 smoothed for the lidar due to the 1-h data-acquisition time. At 3.3 km 250 ppm corresponds to roughly 5 % RH.  
 908

909

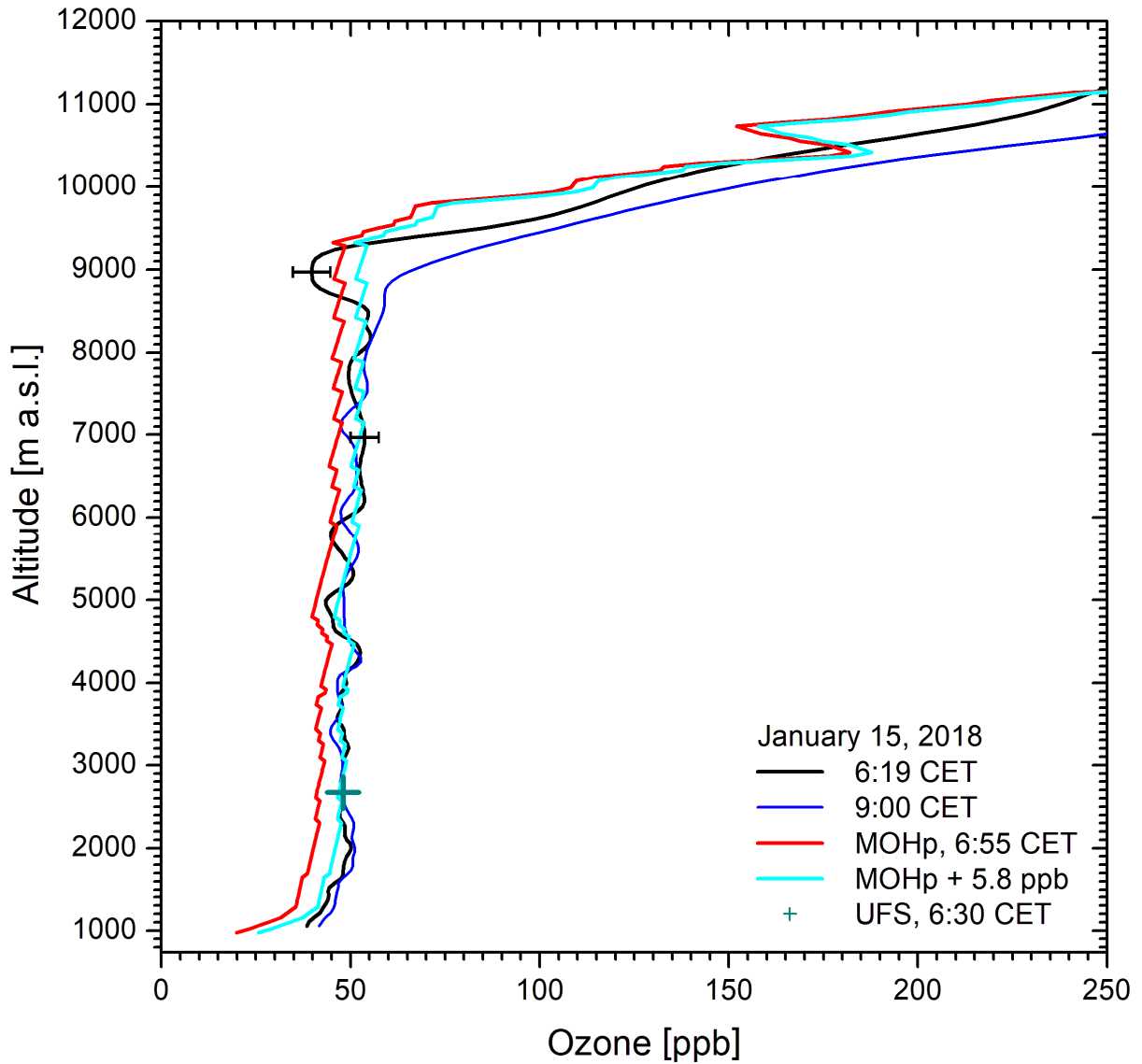


910 **Fig. 3.** Averaged differences between FZJ ozone sonde and IMK-IFU lidar for the first three comparisons after a  
911 slight offset correction of the sonde profiles (see text)

912

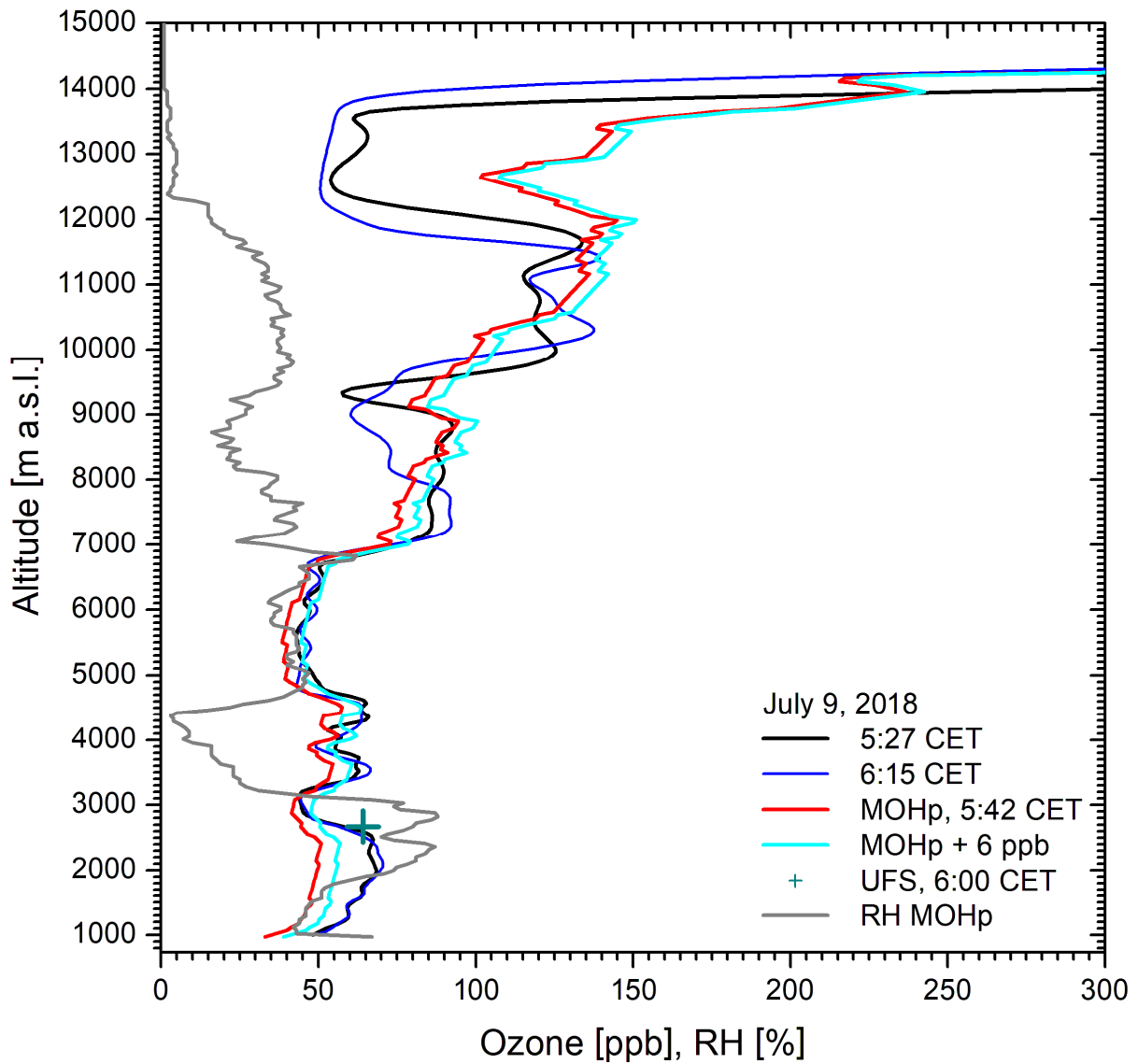
913

914



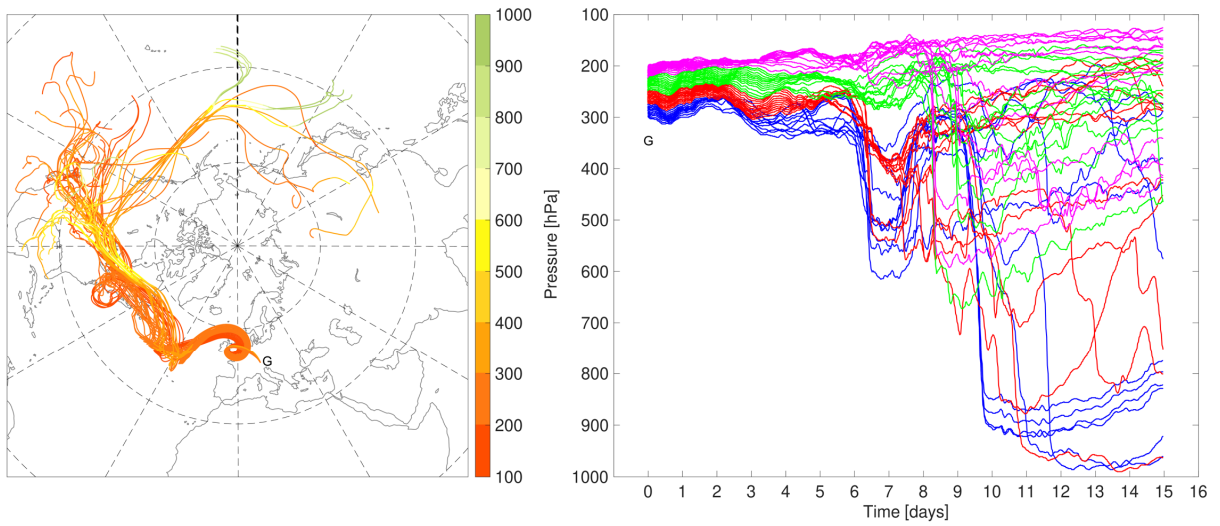
916 **Fig. 4.** Ozone measurements on 15 January 2018: The MOHp ozone (red) is also shown shifted by 5.8 ppb to  
 917 match the lidar ozone (cyan), in part the black, in part the blue curve. Differences exist in the tropopause region,  
 918 which is frequently the case. The sawtooth structure in the MOHp data is due to insufficient digital resolution in  
 919 the NDACC data base.  
 920

921



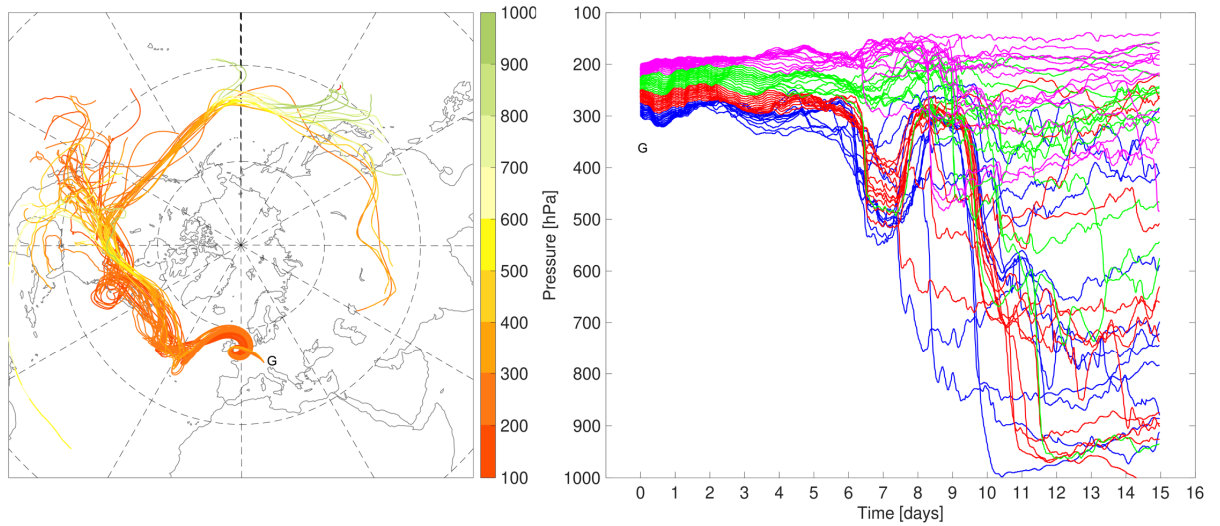
922 **Fig. 5.** Summertime ozone measurements (July 9, 2018) with pronounced layering; the sonde ozone (red) is  
 923 brought to reasonable agreement with the lidar (black curve) above 2.7 km by adding 6 ppb (cyan curve). Above  
 924 9 km the air masses are no longer comparable. The particularly strong discrepancy of the UFS in-situ ozone can  
 925 be explained by orographic lifting of the ozone edge at 2.7 km. The moderate RH (grey) in the free troposphere  
 926 indicates that the very high ozone values could be due to a stratospheric air component.  
 927

928



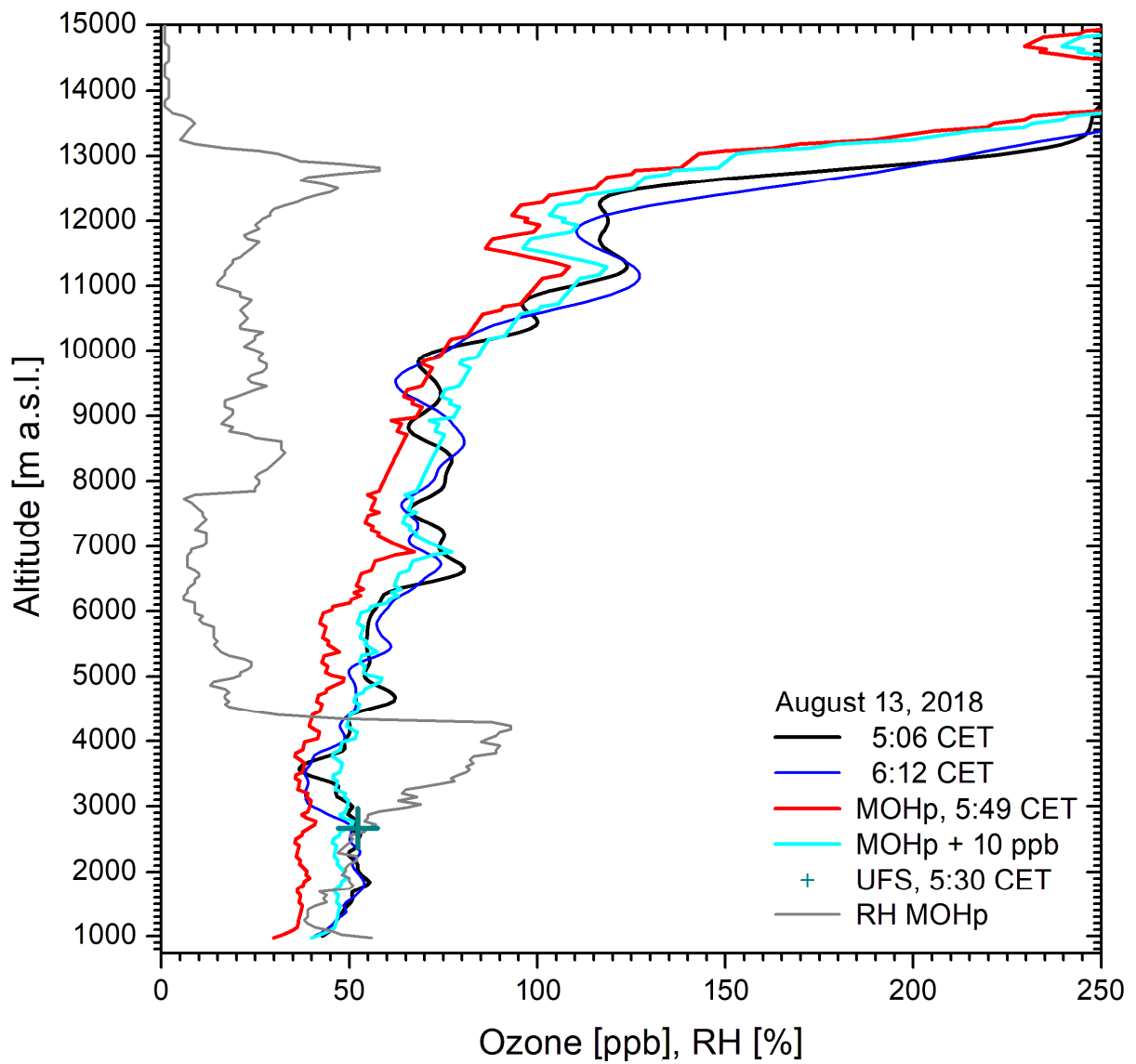
929  
930

**Fig. 6.** 350-h LAGRANTO backward trajectories, started above Garmisch-Partenkirchen (G) on 9 July 2018 at 7:00 CET

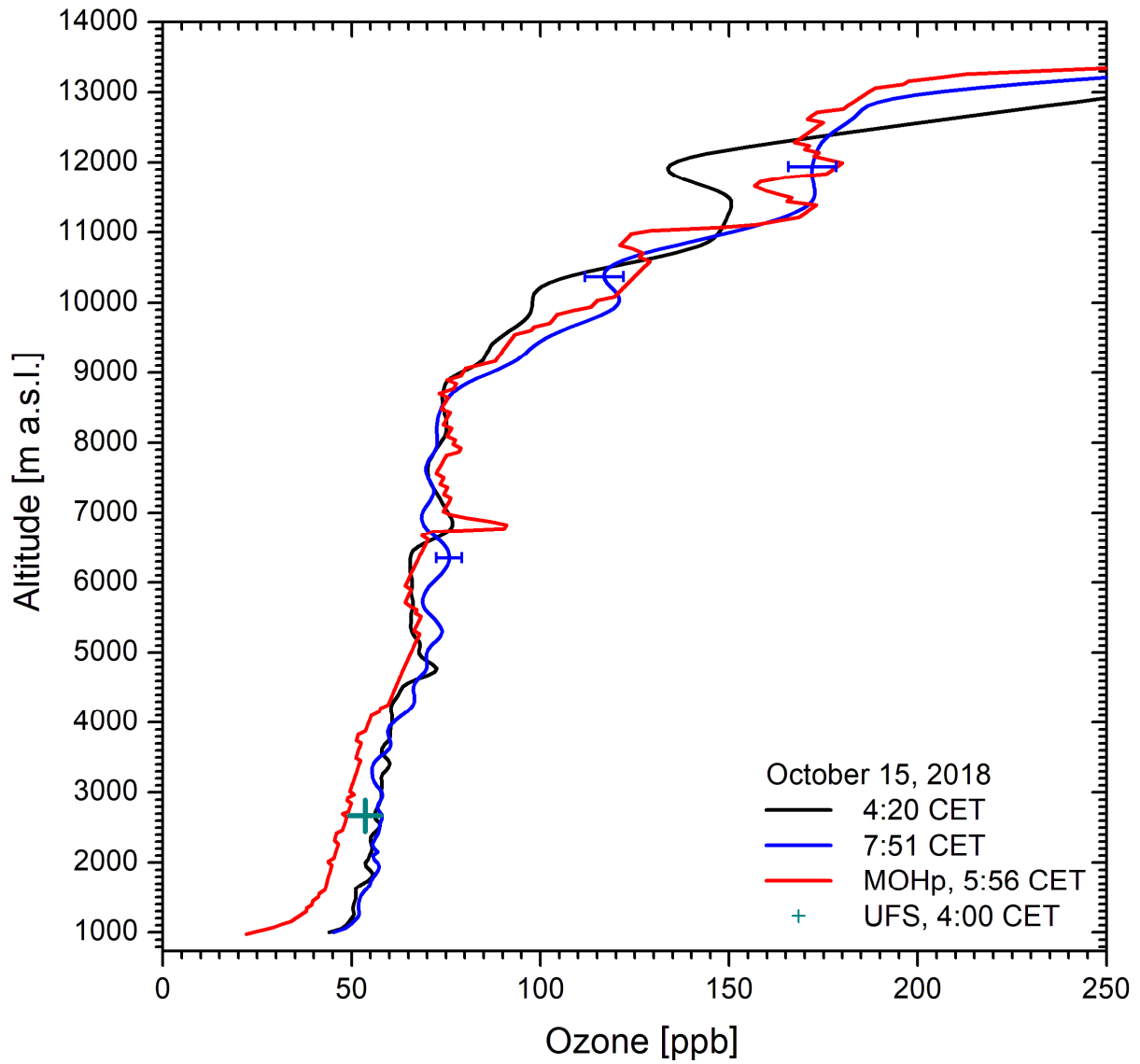


931  
932

**Fig. 7.** 350-h LAGRANTO backward trajectories, started above Garmisch-Partenkirchen (G) on 9 July 2018 at 8:00 CET



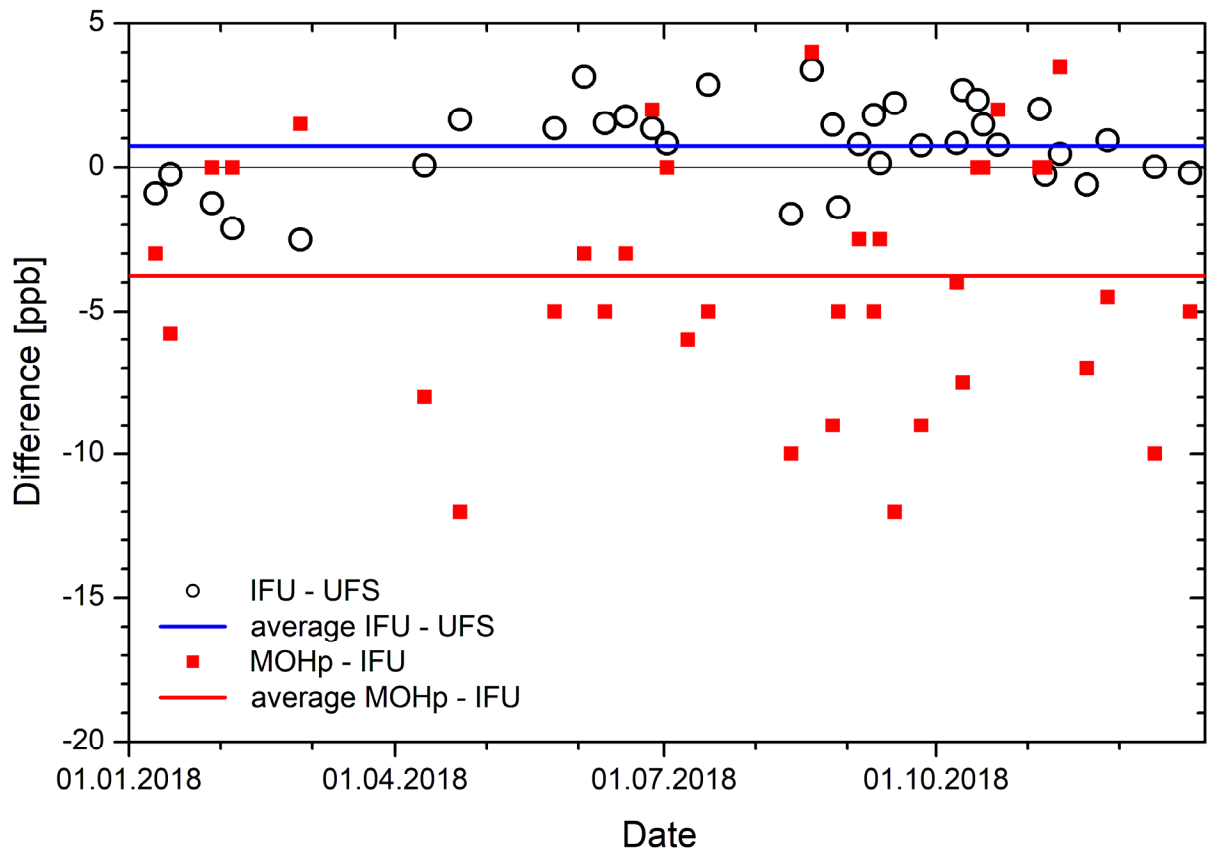
934 **Fig. 8.** Ozone measurements on 13 August 2018: The agreement of the shifted MOHp ozone profile (cyan) with  
 935 the lidar curves is rather good up to 12 km given the high summertime variability. The low to moderate RH  
 936 above 4.4 km (grey) indicates that the elevated ozone is partially caused by stratospheric air.  
 937



939 **Fig. 9.** Ozone measurements on 15 October 2018: The MOHp ozone (red) is not shifted. The agreement above  
 940 4.3 km is better with the earlier lidar measurement (black), above 7 km better with the blue curve. The lidar data  
 941 are strongly smoothed in the stratosphere, as can be seen from the more detailed ozone structure in the sonde  
 942 data. This example is one of the two examples with a pronounced low-altitude discrepancy between lidar and  
 943 sonde extending to more the 3 km.

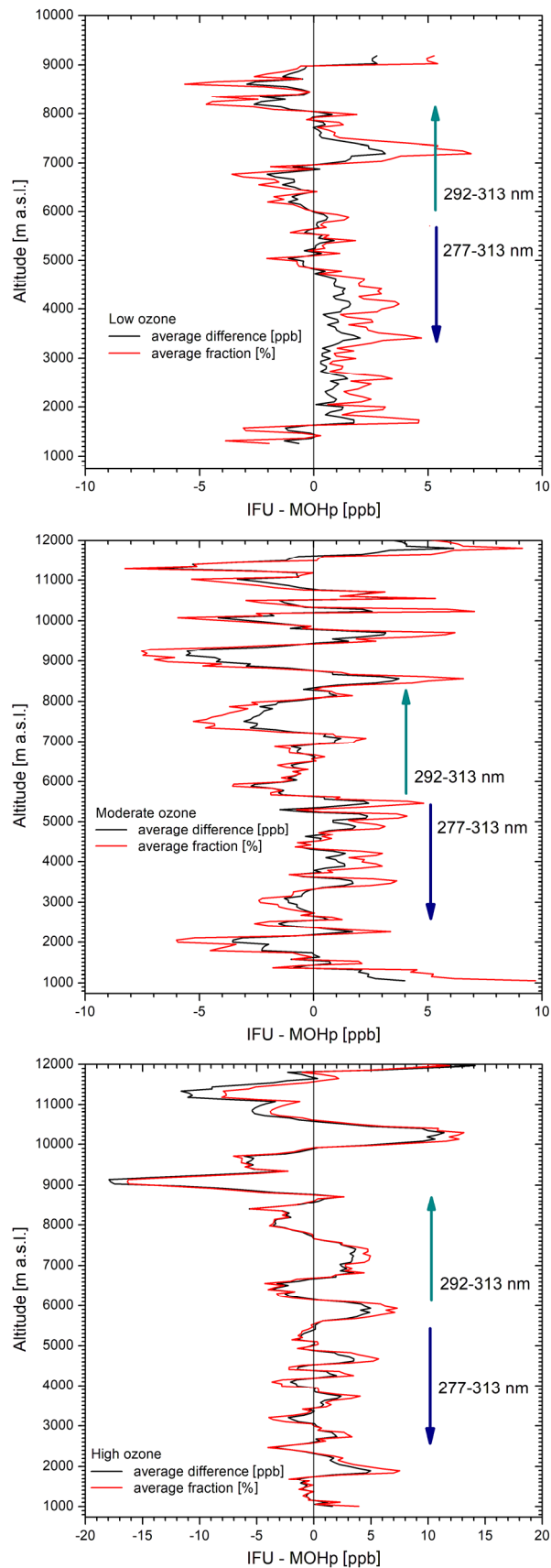
944

945



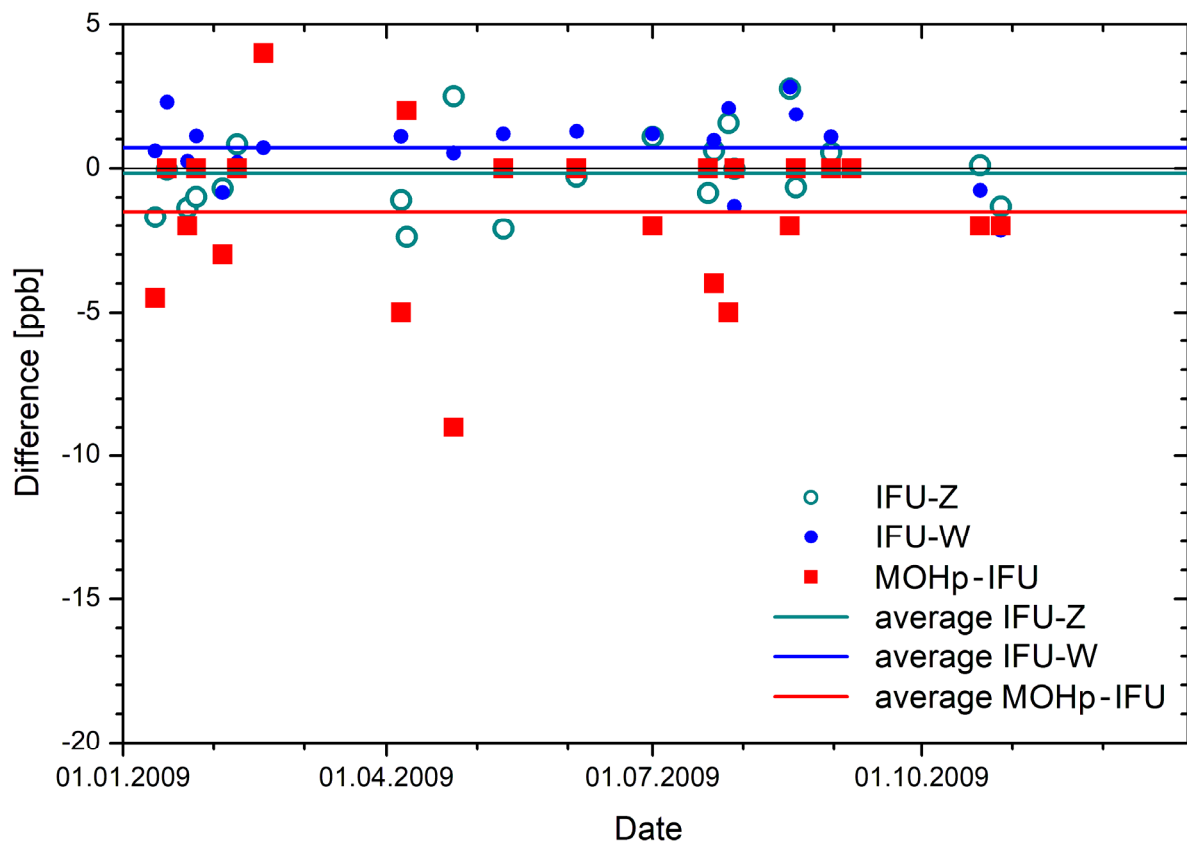
946 **Fig. 10.** Differences between the ozone values of the IFU DIAL at 2670 m and the UFS routine measurements as  
947 well as the offsets of the MOHp profiles with respect to the DIAL for 35 of the 36 measurement days of the 2018  
948 comparison. The blue curve represents a  $\pm 2$ -point running average of the differences between lidar and station.  
949





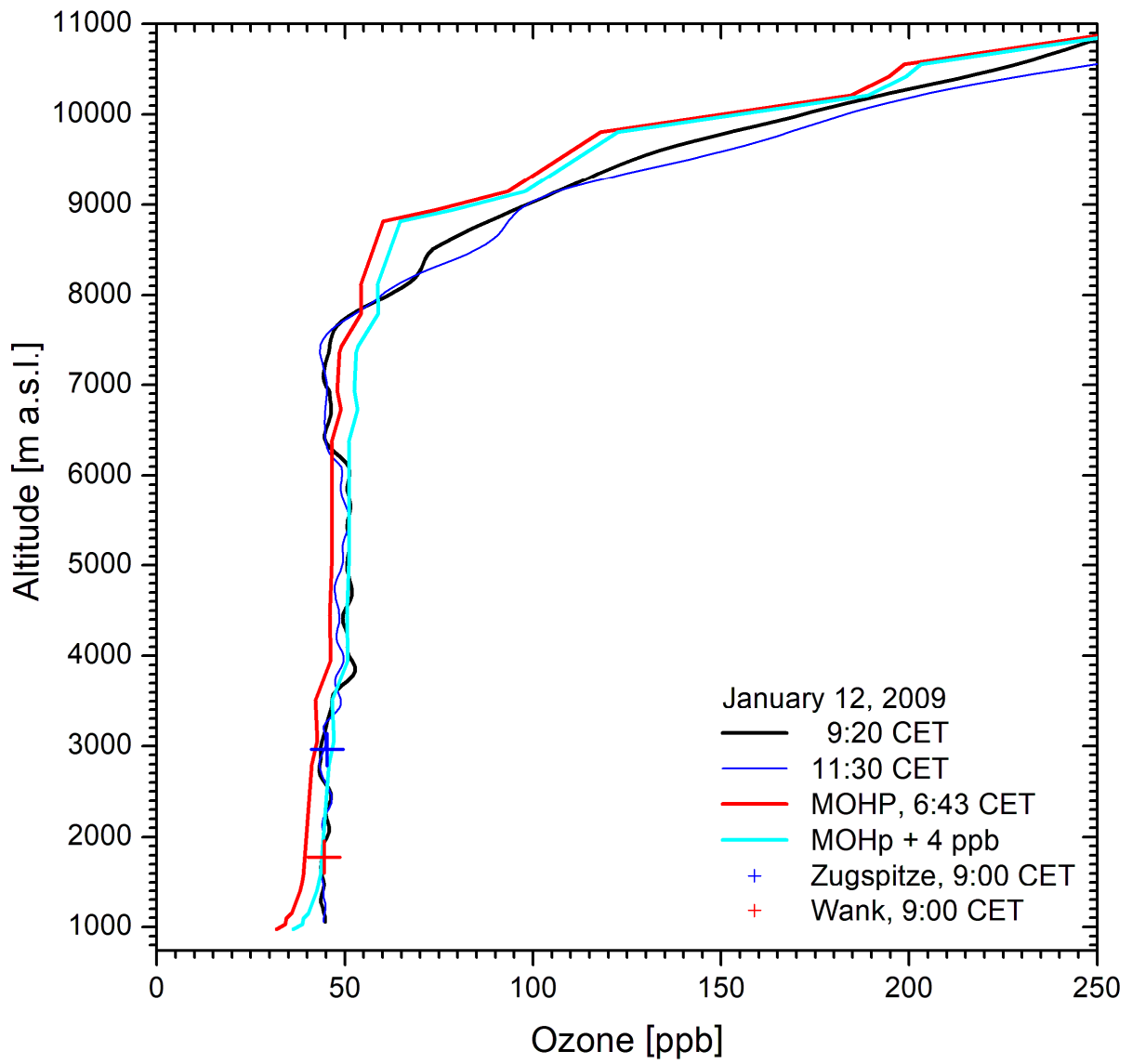
951 **Fig. 11.** Average differences between IFU lidar and offset-corrected MOHp sonde in 2018 for low-, moderate  
 952 and high-conditions (based on six, seven and six comparisons, respectively); the uncertainties may be estimated  
 953 from the maximum differences around the respective altitudes. We also indicate the approximate altitude ranges  
 954 of the two wavelength pairs used for the lidar data evaluation.

956



957 **Fig. 12.** Differences between the ozone mixing ratios of the lidar (IFU) and the stations Zugspitze (Z), Wank  
958 (W) at the summit altitudes, and offsets between lidar and MOHp sonde for 2009  
959

960



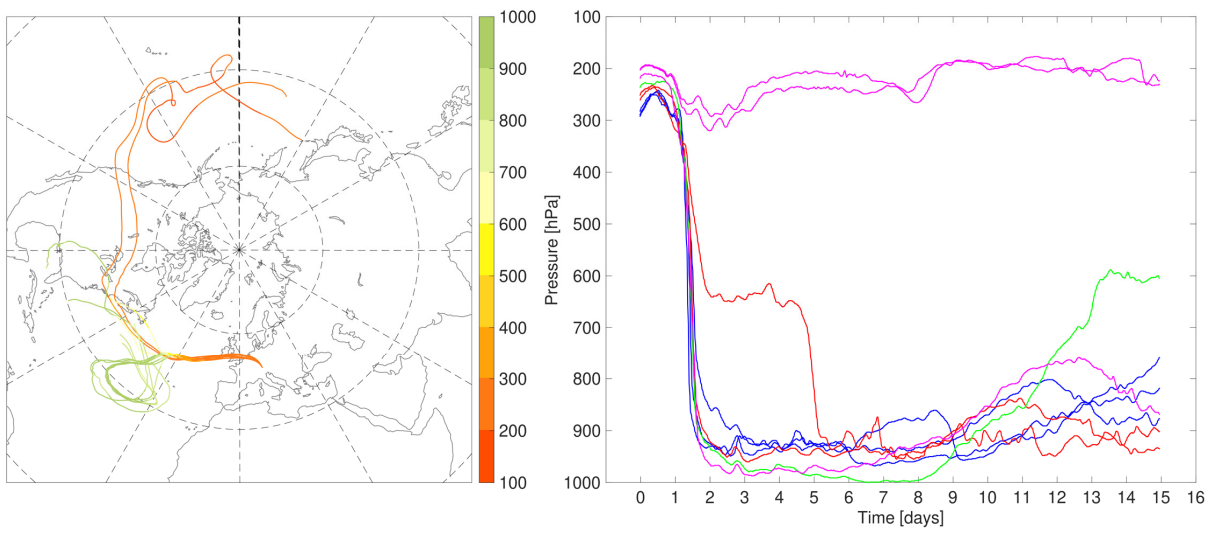
961 Fig. 13. Ozone measurements on 12 January 2009

962



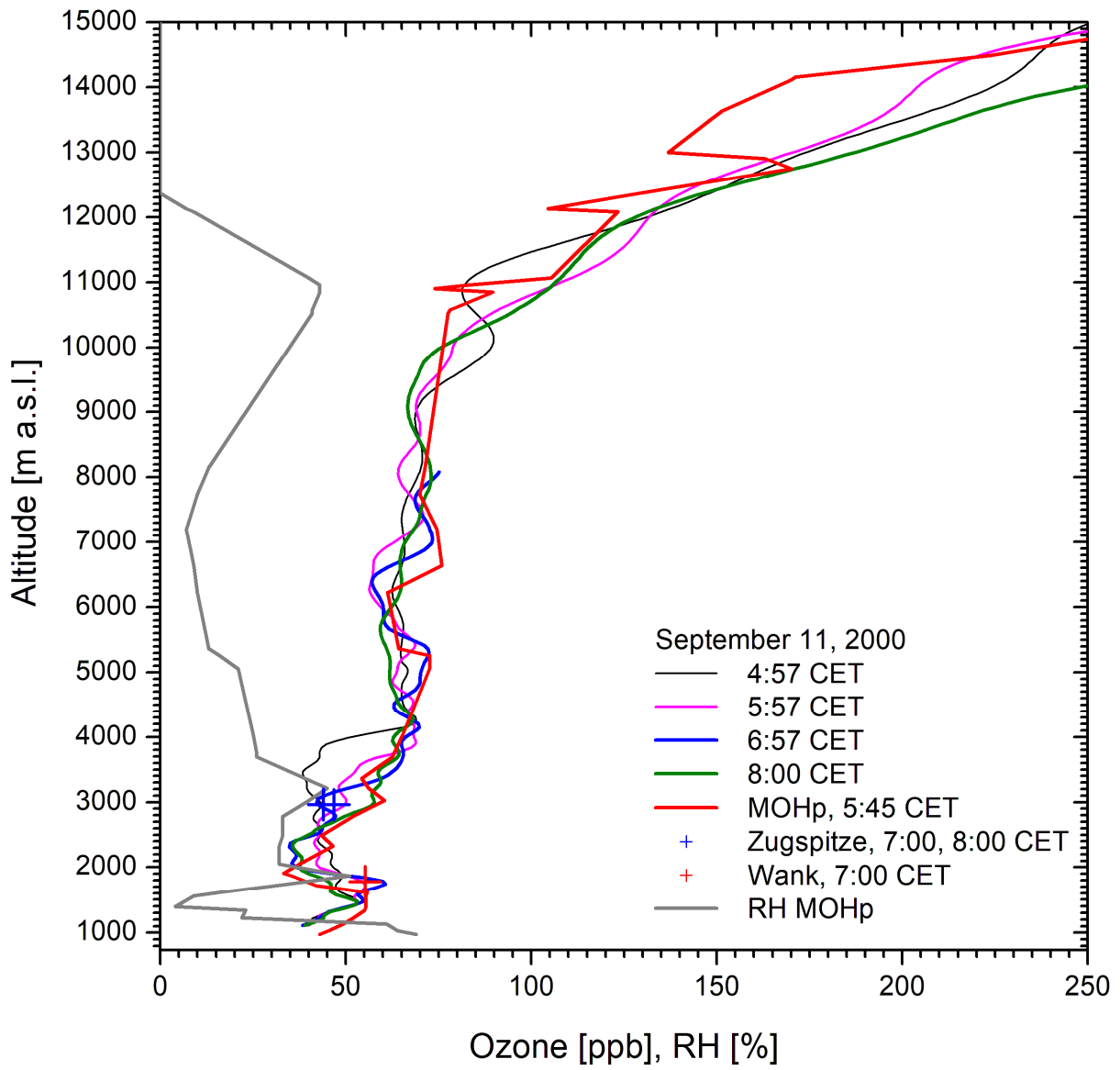
964 **Fig. 14.** Ozone measurements on 17 August 2009; the structure in the upper troposphere is strongly influenced  
 965 by smoothing. The bias between 5.5 and 8 km has not been explained.  
 966

967



968 **Fig. 15.** 350-h LAGRANTO backward trajectories, started above Garmisch-Partenkirchen (G) on 9 July 2018 at  
969 7:00 CET  
970

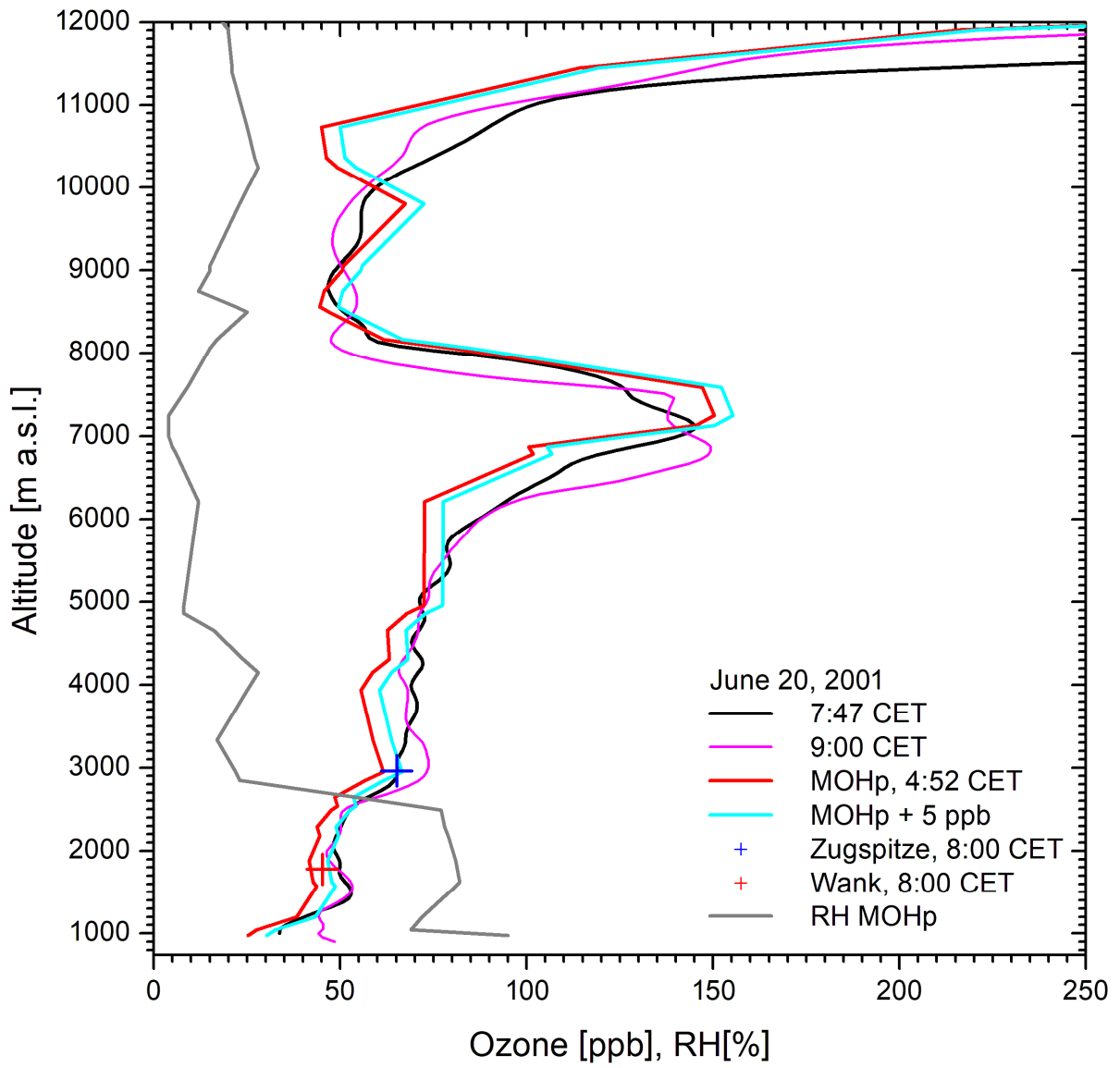
971



972 **Fig. 16.** Ozone measurements on 11 September 2000; in this case no offset was determined.

973

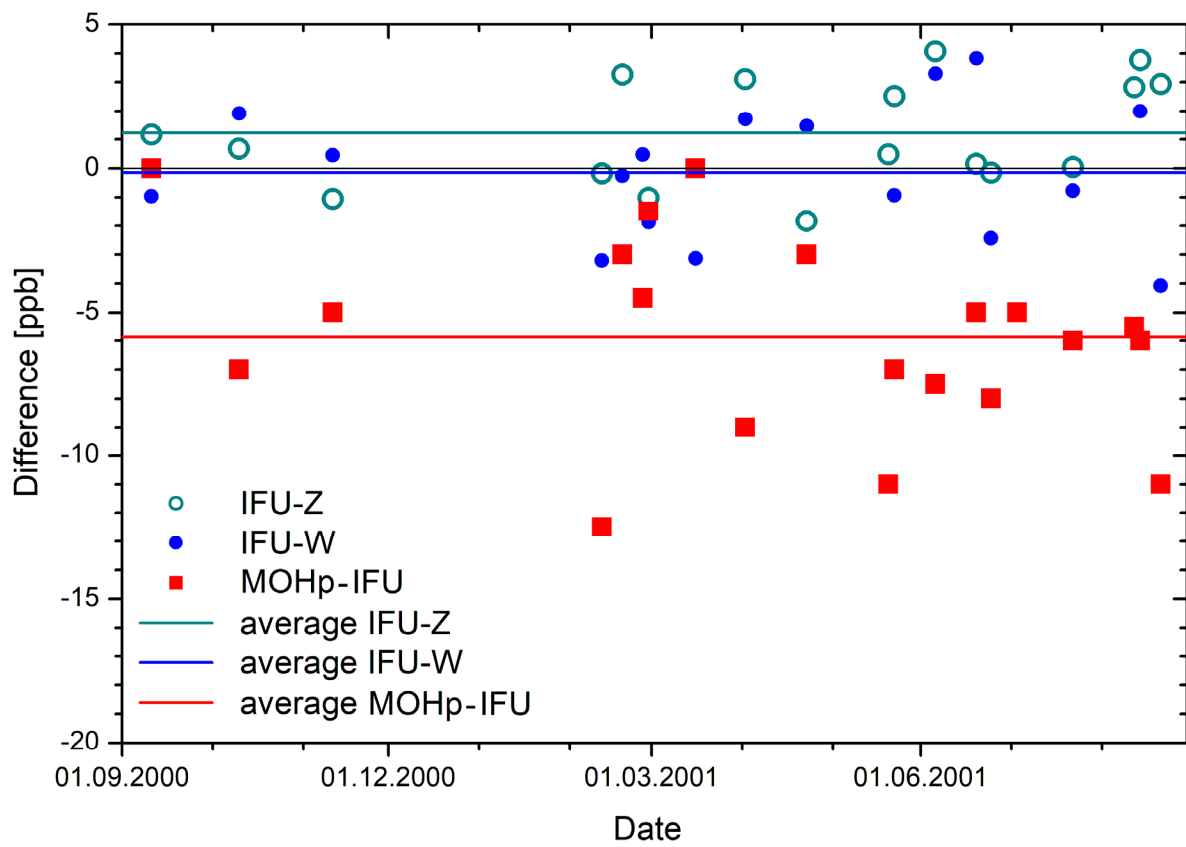
974



975 Fig. 17. Ozone measurements on 20 June, 2001

976

977



978 **Fig. 18.** Differences between the ozone mixing ratios of the lidar (IFU) and the stations Zugspitze (Z), Wank  
979 (W) at the summit altitudes, and between lidar and MOHp sonde, determined by shifting the sonde profile, for  
980 2009.